ISSUE ON ACOUSTIC SOURCE LOCALIZATION AND TRACKING IN DYNAMIC REAL-LIFE SCENES

◆IEEE

(Contents Continued from Page 1)

Subspace-Based Algorithms for Localization and Tracking of Multiple Near-Field Sources

Weiliang Zuo, Jingmin Xin 🅞 , *Senior Member, IEEE*, Hiromitsu Ohmori, *Member, IEEE*,
Nanning Zheng, *Fellow, IEEE*, and Akira Sano, *Member, IEEE*

Abstract—In this paper, we investigate the problems of estimating and tracking the location parameters [i.e., directions-of-arrival (DOAs) and ranges] of multiple near-field (NF) narrow-band sources impinging on a symmetric uniform linear array, and a simple subspace-based algorithm for localization of NF sources (SALONS) is presented, where the computationally burdensome eigendecomposition and spectrum peak searching are avoided. In the SALONS, the DOAs and ranges are estimated separately with a one-dimensional subspace-based estimation technique, where the null spaces are obtained through the linear operation of the correlation matrices formed from the antidiagonal elements of the noiseless array covariance matrix, and the estimated DOAs and ranges are automatically paired without any additional procedure. Then the statistical analysis of the presented batch SALONS is studied, and the asymptotic mean-squared-error expressions of the estimated DOAs and ranges are derived. Furthermore, an online algorithm is developed for tracking the multiple moving NF sources with crossover points on their trajectories. The effectiveness and the theoretical analysis of the presented algorithms are verified through numerical examples, and the simulation results show that the proposed algorithms provide good estimation and tracking performance for DOAs and show satisfactory estimation and tracking performance for ranges.

Index Terms—Linear operation, near-field, source localization, uniform linear array.

I. INTRODUCTION

SOURCE localization and tracking play important roles in many applications of sensor array processing such as sonar, collision avoidance radar, electronic surveillance, seismology, speech enhancement, speaker localization using microphone arrays, and biomedical imaging (e.g., [1]–[15] and references

therein). Unlike the case of signal sources in the far-field (FF), where the wave emanated from the signal source is considered as the plane-wave at the array and characterized by the direction-of-arrival (DOA) only, and the range (i.e., distance) becomes irrelevant, when the signal source is close to the array and lies in the near-field (NF) (i.e., the Fresnel region), the wave imping-ing on the array has the spherical wavefront characterized by two independent location parameters (i.e., the DOA and range). In past decades, numerous methods were proposed for the spherical wavefront model (e.g., [23]–[27]), for examples, the modified two-dimensional (2D) MUSIC [23], the polynomial rooting approach [24], the maximum-likelihood (ML) location estimator [25], the MUSIC curved wavefront (MCW) algorithm [26], and the spherical harmonics domain method [27]. However, most of these methods involve multidimensional searching or high-order Taylor series expansion and have high computational loads.

In order to facilitate the problem of NF source localization, the nonlinear propagation time delay of the spherical wavefront model can be approximated into a quadratic wavefront model with its second-order Taylor expansion (i.e., Fresnel approximation) [28]. As a result, some localization methods were proposed for the NF narrowband sources [29]–[35], for instance, the path-following methods [29], [30], the high-order statistics (HOS) or cyclostationarity based methods [31]–[34]. In contrast to the aforementioned methods based on the traditional spherical wavefront model [23]–[27], these quadratic wavefront approximation based methods usually require low computational efforts, but they suffer some systematic estimation errors of location parameters introduced by the Fresnel approximation [36], and the linear antenna array based method [35] is only suitable for a single NF source, while some correction methods were considered to mitigate the systematic error [37], [71]. Additionally the NF source localization problem was extended and dealt with the bistatic multiple-input multiple-output (MIMO) radar systems by utilizing the approximated model of time delay [72], [73] or the exact model of time delay [74]–[77] with linear arrays in 2D space or with arbitrary planar arrays in 3D space, while several 3D localization methods were also reported for a single NF source with uniform circular array [78], [79].

Furthermore the matrix-form expressions of the stochastic (i.e., unconditional) Cramer-Rao lower bounds (CRBs) were presented for multiple NF sources [24], [44], and some nonmatrix-form analytical expressions of the deterministic (i.e., conditional) CRBs were derived for one single time-varying NF source [80], [81] and two NF sources [82], [83], while several

different deterministic lower bounds were also derived for characterizing the non-asymptotic performance of one single NF source [84]. By using the exact model of time delay, the "exact" closed-form expressions of the stochastic and deterministic CRBs were derived for one single NF source impinging on the uniform linear array (ULA) [85], [86], the arbitrary linear arrays [38], the uniform circular array [87], and the planar array [88].

Recently by utilizing the geometric configuration of centrosymmetric linear arrays [38] and the quadratic wavefront approximation model, many HOS (or cyclostationarity) and second-order statistic (SOS) based localization methods were developed for the NF sources [39]–[49]. Among them, the HOS (or cyclostationarity) based methods [39]–[42] often involve multidimensional searching or are suitable only for the incident signals with specifically temporal properties, and they require many array snapshots and have high computational load, while the SOS-based methods [43]–[49] are more computationally efficient compared to the former. However, the generalized ESPRIT and MUSIC based method (GEMM) [45] performs worse for finite array snapshots, because the generalized ESPRIT [53] encounters ambiguity in some scenarios owing to the selection of weighting matrix [54], while the rank reduction based method [47] generally performs better than the GEMM with more computational load [55]. The reduced-dimension MUSIC algorithm (RD-MUSIC) [48] obtains the DOA estimates by 1D peak-searching procedure, which is really time-consuming. Although the weighted linear prediction method (WLPM) [44] has a rather simple way to implement, the structure property of the array covariance matrix of the incident signals is required in these methods [43], [44], [46], where this structure property is only valid for large number of snapshots. Additionally the sparse recovery method has a rather difficulty to determine the regularization parameter that balances the tradeoff between the Frobenius norm term and ℓ_1-norm term in the objective function [49]. On the other hand, an adaptive algorithm was suggested [50], it still requires the eigendecomposition, which is rather computationally intensive and time-consuming, and consequently this algorithm is unsuitable for some practical situations, when the number of sensors is large and/or the trajectories of multiple moving NF sources have crossover points (cf. [51], [52] and references therein).

On the other hand, the problem of tracking multiple moving sources is very important in practical applications of radar, sonar, communications, and so on (cf. [68]), and many on-line algorithms have been widely studied for tracking the 1D DOA or 2D DOAs (i.e., azimuth and elevation angles) of multiple FF sources from different viewpoints (see, e.g., [52], [65], [66], [92], [93], [96], [97], [64] and references therein). Similarly to the 2D DOA tracking of multiple FF sources (cf. [66]), multiple successively estimated location parameters (i.e., DOAs and ranges) obtained at different time instants should be pair-matched for the same source, and this association becomes considerably more difficult than the 1D tracking of multiple FF sources due to the increase in the dimensionality. To the best of our knowledge, the tracking of NF narrowband sources with uniform sensor arrays has not been considered in the literature of array processing except the fuzzy neural networks (FNN) based method [108] and the

fast simulated annealing (FSA) and adaptive simulated annealing (ASA) algorithms [109]. However, the FNN-based method [108] was developed with ULA for a single NF source and inapplicable for multiple moving sources, while the FSA and ASA algorithms with randomly distributed sensors [109] model each source as a first-order autoregressive process and require an iteration procedure to accomplish search strategy for the global minimum, which is computationally intensive.

Therefor in this paper, we investigate the problems of localizing and tracking multiple NF narrowband sources impinging on a symmetric ULA. Motivated by the subspace-based localization of FF and NF sources without eigendecomposition (LOFNS) [70], we present a simple subspace-based algorithm for localization of NF sources (SALONS) by utilizing the anti-diagonal elements of the noiseless array covariance matrix. In the SALONS, the DOAs and ranges are estimated separately with a 1D subspace-based estimation technique, where the null spaces are obtained through a linear operation of the correlation matrices formed from the anti-diagonal elements of the noiseless array covariance matrix, and the estimated DOAs and ranges are automatically paired without any additional procedure, where the computationally burdensome eigendecomposition and spectrum peak searching are avoided. Then the statistical property of the batch SALONS is analyzed, and the asymptotic mean-squared-error (MSE) expressions of the estimation errors are derived for both the estimated DOAs and ranges. Furthermore, an on-line algorithm is developed for tracking multiple moving NF sources with crossover points on their trajectories. The effectiveness and the theoretical analysis of the proposed algorithms are substantiated through numerical examples, and the simulation results show that the batch and adaptive algorithms provide good estimation and tracking performance for both the DOAs and ranges.

Remark A: In fact, the FF sources and the NF sources may coexist in some practical scenarios (for example, speaker localization with microphone arrays) (e.g., [98]–[100]), and hence many different methods were developed for the localization of these mixed sources (see, e.g., [101]–[106], [70] and the references therein), where the stochastic CRB and the SNR threshold were investigated in [102] and [107], respectively. In our previous work, the so-called LOFNS was proposed for localizing the mixed FF and NF sources impinging on the symmetric ULA [70], where the oblique projection operator (see, e.g., [63]) is utilized to isolate the NF signals from the FF ones, and the procedures of computationally burdensome eigendecomposition are not required in the estimation of the NF and FF location parameters and the computation of oblique projection operator. Unfortunately, the problem of tracking NF and FF sources is much complicated, and this problem has not been studied in the literature of array processing. □

Notation: In the paper, $\boldsymbol{O}_{m\times n}$, $\boldsymbol{I}_m$, $\boldsymbol{0}_{m\times 1}$, and $\delta_{n,t}$ stand for an $m\times n$ null matrix, $m\times m$ identity matrix, $m\times 1$ null vector, and Kronecker delta, and $E\{\cdot\}$, $\{\cdot\}^*$, $(\cdot)^T$, and $(\cdot)^H$ represent the statistical expectation, complex conjugate, transposition, and Hermitian transposition, respectively. Additionally, $(\cdot)^\dagger$ and $\mathrm{diag}(\cdot)$ denote Moore-Penrose pseudoinverse and the diagonal matrix operator, while $\mathcal{R}(\cdot)$ and $\mathcal{N}(\cdot)$ indicate the
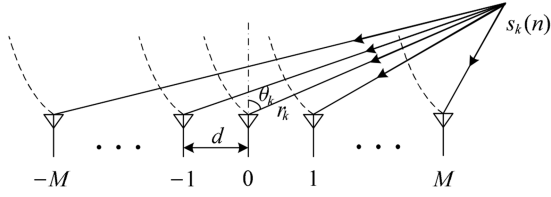
Fig. 1.   The localization of near-field source signals with a symmetric ULA.

range space or null space of the bracketed matrix. Furthermore, $\otimes$, $\oplus$, and $\text{tr}\{\cdot\}$ signify the Kronecker product, the direct sum operator, and the trace operator, and $\text{Im}\{\cdot\}$ and $\text{Re}\{\cdot\}$ denote the imaginary or real part of the bracketed quantity, while $\boldsymbol{e}_i$ is a $(2M+1) \times 1$ unit vector with a unity element

II. DATA MODEL

We consider K signals $\{s_k(n)\}$ from the NF narrowband sources impinging on a ULA consisting of $2M+1$ sensors with spacing d as depicted in Fig. 1, where the sensors are assumed to be fully calibrated, and the center of the array is assumed as the phase reference point. The received noisy signal $x_i(n)$ at the ith sensor can be expressed as

$$x_i(n) = \sum_{k=1}^{K} s_k(n) e^{j\tau_{ik}(n)} + w_i(n) \qquad (1)$$

for $i = -M, \ldots, -1, 0, 1, \ldots, M$, where n denotes the discrete time instant, $w_i(n)$ is the additive noise, and $\tau_{ik}(n)$ is the phase delay due to the time delay between the reference sensor and the ith sensor for the kth incident signal $s_k(n)$, which is given by (cf. [28])

$$\tau_{ik}(n)$$
$$= \frac{2\pi}{\lambda} \left(\sqrt{r_k^2(n) + (id)^2 - 2idr_k(n)\sin\theta_k(n)} - r_k(n) \right) \qquad (2)$$

where $\theta_k(n)$ and $r_k(n)$ are the DOA and range of $s_k(n)$, and λ is the wavelength. When the signal $s_k(n)$ is in the Fresnel region (i.e., $r_k(n) \in (0.62(D^3/\lambda)^{1/2}, 2D^2/\lambda)$), where D is the aperture of the array given by $D = 2Md$ herein (cf. [4]), $\tau_{ik}(n)$ in (2) can be approximated with the second-order Taylor expansion as [28], [44]

$$\tau_{ik}(n) \approx i\psi_k + i^2\phi_k \qquad (3)$$

in which ψ_k and ϕ_k are the electric angles defined by

$$\psi_k \triangleq -\frac{2\pi d}{\lambda} \sin(\theta_k(n)) \qquad (4)$$

$$\phi_k \triangleq \frac{\pi d^2}{\lambda r_k} \cos^2(\theta_k(n)). \qquad (5)$$

Then the received signals can be rewritten compactly

$$\boldsymbol{x}(n) = \boldsymbol{A}\boldsymbol{s}(n) + \boldsymbol{w}(n) \qquad (6)$$

where $\boldsymbol{x}(n) \triangleq [x_{-M}(n), \ldots, x_{-1}(n), x_0(n), x_1(n), \ldots, x_M(n)]^T$, $\boldsymbol{s}(n) \triangleq [s_1(n), s_2(n), \ldots, s_K(n)]^T$, and $\boldsymbol{w}(n) \triangleq [w_{-M}(n), \ldots, w_{-1}(n), w_0(n), w_1(n), \ldots, w_M(n)]^T$, while $\boldsymbol{A}$

is the array response matrix defined by $\boldsymbol{A} \triangleq [\boldsymbol{a}(\theta_1(n), r_1(n)), \boldsymbol{a}(\theta_2(n), r_2(n)), \ldots, \boldsymbol{a}(\theta_K(n), r_K(n))]$, and $\boldsymbol{a}(\theta_k(n), r_k(n)) \triangleq [e^{-jM\psi_k}e^{jM^2\phi_k}, \ldots, e^{-j\psi_k}e^{j\phi_k}, 1, e^{j\psi_k}e^{j\phi_k}, \ldots, e^{jM\psi_k}e^{jM^2\phi_k}]^T$.

Here we make the basic assumptions as follows.

A1) The array is calibrated, and the array response matrix $\boldsymbol{A}$ has full rank and is unambiguous (i.e., $\text{rank}\{\boldsymbol{A}\} = K$).

A2) The incident signals $\{s_k(n)\}$ are temporally complex white Gaussian random processes with zero-mean and the variance given by $E\{s_k(n)s_k^*(t)\} = r_{s_k}\delta_{n,t}$ and $E\{s_k(n)s_k(t)\} = 0, \forall n, t$.

A3) The additive noises $\{w_i(n)\}$ are temporally and spatially complex white Gaussian random processes with zero-mean and the covariance matrices $E\{\boldsymbol{w}(n)\boldsymbol{w}^H(t)\} = \sigma^2\boldsymbol{I}_{2M+1}\delta_{n,t}$, and $E\{\boldsymbol{w}(n) \cdot \boldsymbol{w}^T(t)\} = \boldsymbol{O}_{(2M+1)\times(2M+1)}, \forall n, t$. In addition, the additive noises are independent to the incident signals, i.e., $E\{\boldsymbol{s}(n)\boldsymbol{w}^H(n)\} = E\{\boldsymbol{s}(n)\boldsymbol{w}^T(n)\} = \boldsymbol{O}_{K\times(2M+1)}$.

A4) The number of incident signals K is known, and K satisfies the relation $K < M+1$.

A5) The sensor spacing d satisfies the relation $d \leq \lambda/4$ for avoiding the estimation ambiguity.

In the following, we concentrate on the estimation and tracking of location parameters $\{\theta_k(n)\}_{k=1}^{K}$ and $\{r_k(n)\}_{k=1}^{K}$ of multiple NF source signals from the finite noisy array data $\{\boldsymbol{x}(n)\}_{n=1}^{N}$.

III. BATCH SOURCE LOCALIZATION: SALONS

Firstly we consider a new computationally efficient subspace-based and batch method for estimating the DOAs and ranges of multiple NF sources, where the source locations are time invariant, i.e., $\theta_k(n) = \theta_k(n) = r_k$, and this will be a base for source tracking developed in Section IV.

A. Subspace Estimation

Under the basic assumptions, from (6), we obtain the $(2M+1) \times (2M+1)$ array covariance matrix $\boldsymbol{R}$

$$\boldsymbol{R} \triangleq E\{\boldsymbol{x}(n)\boldsymbol{x}^H(n)\} = \boldsymbol{A}\boldsymbol{R}_s\boldsymbol{A}^H + \sigma^2\boldsymbol{I}_{2M+1} \qquad (7)$$

where $\boldsymbol{R}_s \triangleq E\{\boldsymbol{s}(n)\boldsymbol{s}^H(n)\} = \text{diag}(r_{s_1}, r_{s_2}, \ldots, r_{s_K})$. We can express its pqth element $(\boldsymbol{R})_{pq}$ along the major anti-diagonal (for $m = 0$) and that along the mth ($1 \leq |m| < M$) upper (for $m > 0$) or lower (for $m < 0$) diagonal off the major anti-diagonal as

$$(\boldsymbol{R})_{pq} \triangleq E\{x_p(n)x_q^*(n)\}$$
$$= \sum_{k=1}^{K} r_{s_k} e^{j(2p+m)\gamma_{mk}} + \sigma^2\delta_{p,-p-m} \triangleq \rho_m(p) \qquad (8)$$

for $p = -M + m_2, -M + m_2 + 1, \ldots, -1, 0, 1, \ldots, M - m_1 - 1, M - m_1$, and $q = -p - m$, where $m_1 = 0.5(|m| + m)$, $m_2 = 0.5(|m| - m)$, and $\gamma_{mk} \triangleq \psi_k - m\phi_k$. By partitioning

the matrix R in (7) into four submatrices as

$$R = \begin{bmatrix} R_{11}, & R_{12} \\ R_{21}, & R_{22} \end{bmatrix} \begin{matrix} K \\ 2M+1-K \end{matrix} \qquad (9)$$

we have the noise variance σ^2 from R_{21} and R_{22} as [57]

$$\sigma^2 = \frac{\mathrm{tr}\{R_{22}\Pi\}}{\mathrm{tr}\{\Pi\}} \qquad (10)$$

where $\Pi \triangleq I_{2M+1-K} - R_{21}R_{21}^\dagger$, and $R_{21}^\dagger = (R_{21}^H R_{21})^{-1}$ $\cdot R_{21}^H$. Hence from (8) and (10), we get the noiseless correlation $\bar{\rho}_m(p)$ of the received array data

$$\bar{\rho}_m(p) \triangleq \rho_m(p) - \sigma^2 \delta_{p,-p-m}$$

$$= \sum_{k=1}^{K} r_{s_k} e^{jm\gamma_{mk}} e^{j2p\gamma_{mk}} \triangleq \bar{r}_{ms}^T b_m(p) \qquad (11)$$

where $\bar{r}_{ms} \triangleq [r_{s_1}e^{jm\gamma_{m1}}, r_{s_2}e^{jm\gamma_{m2}}, \ldots, r_{s_K}e^{jm\gamma_{mK}}]^T$, and $b_m(p) \triangleq [e^{j2p\gamma_{m1}}, e^{j2p\gamma_{m2}}, \ldots, e^{j2p\gamma_{mK}}]^T$. Evidently, $\{\bar{\rho}_m(p)\}$ can be interpreted as the received "signals" for a virtual array of $2M+1-|m|$ sensors illuminated by K "signals" $\{r_{s_k}\}$, and these "signals" $\{\bar{\rho}_m(p)\}$ differ only by a phase factor γ_{mk} (cf. [58]).

Consequently by dividing the virtual array into $L = M + 1 - m_{1\alpha}$ overlapping subarrays with $\bar{K} = M + 1 - m_{2\alpha}$ sensors, where $\bar{K} \geq L \geq K$, $m_{1\alpha} = 0.5(|m| + \alpha(m))$, $m_{2\alpha} = 0.5(|m| - \alpha(m))$, and $\alpha(m) = 0.5(1 - (-1)^m)$, i.e., $|m| \leq 2M + 2 - 2K - \alpha(m)$, we can express the correlation vector ζ_{ml} of the lth subarray as

$$\zeta_{ml} \triangleq [\bar{\rho}_m(M - \bar{K} - m_2 - l + 1),$$

$$\bar{\rho}_m(M - \bar{K} - m_2 - l + 2), \ldots, \bar{\rho}_m(M - m_2 - l)]^T$$

$$= [b_m(M - \bar{K} - m_2 - l + 1),$$

$$b_m(M - \bar{K} - m_2 - l + 2), \ldots,$$

$$b_m(M - m_2 - l)]^T \bar{r}_{ms}$$

$$= \bar{A}_m D_m^{M-\bar{K}-m_2-l+1} \bar{r}_{ms} \qquad (12)$$

where $\bar{A}_m \triangleq [b_m(0), b_m(1), \ldots, b_m(\bar{K}-1)]^T$, and $D_m \triangleq \mathrm{diag}(e^{j2\gamma_{m1}}, e^{j2\gamma_{m2}}, \ldots, e^{j2\gamma_{mK}})$. By concatenating (12) for $l = 1, 2, \ldots, L$ and performing some simple manipulations, we obtain a correlation matrix Z_m as

$$Z_m \triangleq [\zeta_{m1}, \zeta_{m2}, \ldots, \zeta_{mL}]^T$$

$$= \tilde{A}_m^* \bar{R}_{ms} D_m^{M-\bar{K}-m_2+1} \bar{A}_m^T \qquad (13)$$

where $\tilde{A}_m \triangleq [b_m(0), b_m(1), \ldots, b_m(L-1)]^T$, and $\bar{R}_{ms} \triangleq \mathrm{diag}(r_{s_1}e^{jm\gamma_{m1}}, r_{s_2}e^{jm\gamma_{m2}}, \ldots, r_{s_K}e^{jm\gamma_{mK}})$.

Under the assumptions, the ranks of two Vandermonde matrices $\tilde{A}_m$ and $\bar{A}_m$ and two diagonal matrices $\bar{R}_{ms}$ and D_m are given by $\mathrm{rank}(\tilde{A}_m) = \min(L, K) = K$, $\mathrm{rank}(\bar{A}_m) = \min(\bar{K}, K) = K$, and $\mathrm{rank}(\bar{R}_{ms}) = \mathrm{rank}(D_m) = K$. Hence the rank of the $L \times \bar{K}$ matrix Z_m in (13) is obtained as $\mathrm{rank}(Z_m) = K$, i.e., the dimension of signal subspace of Z_m equals the number of incident signals K.

Then we can divide the $L \times K$ matrix $\tilde{A}_m^*$ in (13) into two parts as follows:

$$\tilde{A}_m^* = \begin{bmatrix} \tilde{A}_{m1}^* \\ \tilde{A}_{m2}^* \end{bmatrix} \begin{matrix} \}K \\ \}L-K \end{matrix} . \qquad (14)$$

Since $\tilde{A}_{m1}^*$ is a submatrix of the Vandermonde matrix $\tilde{A}_m^*$ with full rank in (14), we can find that $\tilde{A}_{m1}^*$ is invertible and $\mathrm{rank}(\tilde{A}_{m1}^*) = K$ and the rows of $\tilde{A}_{m2}^*$ are a linear combination of linear independent rows of $\tilde{A}_{m1}^*$, equivalently, there is a $K \times (L-K)$ linear operator P_m between $\tilde{A}_{m2}^*$ and $\tilde{A}_{m1}^*$ as [56], [57], [89]–[96]

$$\tilde{A}_{m2}^* = P_m^H \tilde{A}_{m1}^*. \qquad (15)$$

Hence from (13) and (15), by partitioning the matrix Z_m in (13) as $Z_m = [Z_{m1}^T, Z_{m2}^T]^T$, where Z_{m1} and Z_{m2} consist of the first K and the last $L-K$ rows, respectively, the linear operator P_m can be obtained from the noiseless correlation matrix Z_m (cf. [59])

$$P_m = \tilde{A}_{m1}^{-T} \tilde{A}_{m2}^T = (Z_{m1}Z_{m1}^H)^{-1} Z_{m1} Z_{m2}^H. \qquad (16)$$

From (15), we easily get

$$Q_m^H \tilde{A}_m^* = O_{(L-K)\times K} \qquad (17)$$

where $Q_m \triangleq [P_m^T, -I_{L-K}]^T$. Because the $L \times (L-K)$ matrix Q_m has a full rank of $L-K$, the columns of Q_m in fact form the basis for the null space $\mathcal{N}(\tilde{A}_m^*)$ of $\tilde{A}_m^*$, and clearly the orthogonal projector onto this subspace is given by $\Pi_{Q_m} \triangleq Q_m(Q_m^H Q_m)^{-1} Q_m^H$, which implies that [56]

$$Q_m^H a_m^* = 0_{(L-K)\times 1}, \text{ for } \theta = \theta_k \qquad (18)$$

where $a_m(\gamma_{mk})$ is the kth column of the matrix $\tilde{A}_m^*$ given by $a_m(\gamma_{mk}) \triangleq [1, e^{-2j\gamma_{mk}}, \ldots, e^{-j2(L-1)\gamma_{mk}}]^T$. Evidently the DOAs and ranges can be estimated based on the orthogonal property in (18) without any eigendecomposition.

Remark B: By considering the SVD of matrix $\tilde{A}_m^*$, we readily verify that the orthogonal projector Π_{Q_m} can be written as $\tilde{A}_m^* = I_L - \tilde{A}_m^*(\tilde{A}_m^T \tilde{A}_m^*)^{-1} \tilde{A}_m^T$ [21]. $\qquad \square$

B. Location Parameter Estimation

Thus when only finite and noisy array data are available, the array covariance matrix R can be obtained

$$\hat{R} = \frac{1}{N} \sum_{n=1}^{N} x(n) x^H(n) \qquad (19)$$

where N is the number of snapshots. Then from (17), the parameters $\{\gamma_{mk}\}_{k=1}^{K}$ of the K NF sources can be estimated by minimizing the following cost function

$$f(\theta) = a_m^H(\gamma_{mk}) \Pi_{\hat{Q}_m} a_m(\gamma_{mk}) \qquad (20)$$

where

$$\mathbf{\Pi}_{\hat{Q}_m} = \hat{\boldsymbol{Q}}_m \left(\hat{\boldsymbol{Q}}_m^H \hat{\boldsymbol{Q}}_m \right)^{-1} \hat{\boldsymbol{Q}}_m^H$$

$$= \hat{\boldsymbol{Q}}_m \left(\boldsymbol{I}_{L-K} - \hat{\boldsymbol{P}}_m^H \left(\hat{\boldsymbol{P}}_m \hat{\boldsymbol{P}}_m^H + \boldsymbol{I}_K \right)^{-1} \hat{\boldsymbol{P}}_m \right) \hat{\boldsymbol{Q}}_m^H \tag{21}$$

$$\hat{\boldsymbol{P}}_m = \left(\hat{\boldsymbol{Z}}_{m1} \hat{\boldsymbol{Z}}_{m1}^H \right)^{-1} \hat{\boldsymbol{Z}}_{m1} \hat{\boldsymbol{Z}}_{m2}^H \tag{22}$$

and $\hat{\boldsymbol{Q}}_m = [\hat{\boldsymbol{P}}_m^T, -\boldsymbol{I}_{L-K}]^T$, in which $\mathbf{\Pi}_{\hat{Q}_m}$ is calculated by using the matrix inversion lemma implicitly, and the orthonormalization of the matrix $\hat{\boldsymbol{Q}}_m$ is used in $\mathbf{\Pi}_{\hat{Q}_m}$ to improve the estimation performance [56], [59].

From (20), by setting $m = 0$, we can see that the DOAs can be estimated with 1D searching, i.e.,

$$f_0(\theta) = \boldsymbol{a}_0^H(\theta) \mathbf{\Pi}_{\hat{Q}_0} \boldsymbol{a}_0(\theta). \tag{23}$$

Once we have the DOA estimates $\{\hat{\theta}_k\}_{k=1}^K$, by setting $m = \bar{m} \neq 0$, from (20), we have

$$f_{\bar{m}}(\hat{\theta}_k, r) = \boldsymbol{a}_{\bar{m}}^H(\hat{\theta}_k, r) \mathbf{\Pi}_{\hat{Q}_{\bar{m}}} \boldsymbol{a}_{\bar{m}}(\hat{\theta}_k, r) \tag{24}$$

where $1 \leq |\bar{m}| < M$, and the estimated parameters $\hat{\theta}_k$ and $\hat{r}_k$ are paired automatically without any additional processing.

Remark C: In the previously proposed LOFNS for the localization of the mixed NF and FF sources [70], a Toeplitz matrix is constructed with the elements of projected array correlation matrix along the major anti-diagonal (i.e., $m = 0$), and then the DOAs of NF sources are estimated from this Toeplitz matrix through a linear operation (cf. [56]), while the ranges of NF sources are estimated from the whole estimated noiseless array covariance matrix through another linear operation. However in the SALONS motivated by the aforementioned LOFNS, a generalized Toeplitz matrix $\boldsymbol{Z}_m$ in (13) is formed from the elements of the array covariance matrix along its different anti-diagonals (i.e., $m = 0$, and $m = \bar{m} \neq 0$, where $1 \leq |\bar{m}| < M$), and the DOAs and ranges of NF sources can be estimated from this Toeplitz matrix with the aid of a linear operation by choosing different anti-diagonal index m. Furthermore by choosing any two different anti-diagonal indices such as $m = m_1 \neq 0$ and $m = m_2 \neq 0$, where $m_1 \neq m_2$, $1 \leq |\bar{m}_1| < M$, and $1 \leq |\bar{m}_2| < M$, the DOAs and ranges of NF sources could be also estimated, though a procedure of pair-matching is required. □

C. Implementation of Presented SALONS

When the finite array data $\{\boldsymbol{x}(n)\}_{n=1}^N$ are available, the implementation of the batch SALONS for NF localization is summarized as follows:

1) Calculate the sample array covariance matrix $\hat{\boldsymbol{R}}$ with (19).
   . . . . $8(2M + 1)^2 N$ flops
2) Estimate the noise variance σ^2 with (9) and (10), and calculate the noiseless correlation $\hat{\rho}_m(p)$ with (11).
   . . . . $2(2M + 1)^2$ flops
3) Estimate the DOAs $\{\theta_k\}_{k=1}^K$ by finding the phases of the K zeros of the following polynomial $p_0(z)$ closest to the

unit circle in the z-plane with (23)

$$p_0(z) \triangleq \boldsymbol{p}_0^H(z) \mathbf{\Pi}_{\hat{Q}_0} \boldsymbol{p}_0(z) \tag{25}$$

where $\boldsymbol{p}_0(z) \triangleq [1, z^{-1}, \ldots, z^{-(L-1)}]^T$, and $z \triangleq e^{j4\pi d \sin \theta / \lambda}$.

$$.16K^2(M + 1 - K) + 8K(M + 1)(M + 1 - K)$$
$$+ 8K(M + 1 - K)^2 + 8(M + 1)(M + 1 - K)^2$$
$$+ 16K^2(M + 1) + 8(M + 1)^2(M + 1 - K)$$
$$+ 8(M + 1)^2 + 8(M + 1) + \mathcal{O}(K^3) \text{ flops}$$

4) Estimate the ranges $\{r_k\}_{k=1}^K$ by finding the phases of the K zeros of the following polynomial $p_{\bar{m}}(z)$ closest to the unit circle in the z-plane with (24)

$$p_{\bar{m}}(z) \triangleq z^{M+1} \boldsymbol{p}_{\bar{m}}^H(z) \mathbf{\Gamma}^H(\hat{\theta}_k) \mathbf{\Pi}_{\hat{Q}_{\bar{m}}} \mathbf{\Gamma}(\hat{\theta}_k) \boldsymbol{p}_{\bar{m}}(z) \tag{26}$$

where $\boldsymbol{p}_{\bar{m}}(z) \triangleq [1, z^{-1}, \ldots, z^{-(L-1)}]^T$, $\mathbf{\Gamma}(\hat{\theta}_k) \triangleq \text{diag}(1, e^{4j\hat{\psi}_k}, \ldots, e^{2(L-1)j\hat{\psi}_k})$, and $z \triangleq e^{2j\bar{m}\pi d^2} \cdot e^{\cos^2 \hat{\theta}_k / (\lambda r)}$.

$$..16K^2(L - K) + 8KL(L - K) + 8K(L - K)^2$$
$$+ 8L(L - K)^2 + 16K^2 L + 8L^2(L - K)$$
$$+ 8L^2 + 8L + \mathcal{O}(K^3) \text{ flops}$$

The computational complexity of each step above is roughly indicated in terms of the number of flops, where a flop is defined as a floating-point addition or multiplication operation as adopted by MATLAB software. The computational complexity of the SALONS is nearly $\mathcal{O}[(2M + 1)^2 N + (M + 1)^3]$ flops when $2M + 1 \gg K$, which occurs often in the application of NF source localization, where $\mathcal{O}(k)$ denotes the term of order smaller or equal to k. The existing methods such as the RD-MUSIC [48] and the GEMM [45] involve the eigendecomposition to obtain the signal/noise subspace. Moreover the GEMM involves one EVD and two 1D spectrum peak searching, and its computational complexity is roughly $\mathcal{O}[(2M + 1)^2 N + (2M + 1)^3 + (2M + 1)^2 180/\Delta\theta + (2M + 1)^2(2D^2/\lambda - 0.62(D^3/\lambda)^{1/2})/\Delta r]$ flops, where $\Delta\theta$ and Δr are the angular and range grid spacings (e.g., $\Delta\theta = 0.02°$ and $\Delta r = 0.02$). Similarly, the computational complexity of the RD–MUSIC is about $\mathcal{O}[(2M + 1)^2 N + (2M + 1)^3 + (2M + 1)(M + 1)^2 180/\Delta\theta]$ flops. Obviously since the computationally burdensome eigendecomposition procedure and peak searching are avoided, the proposed method is computationally more efficient than these existing methods.

Remark D: As shown in Fig. 2, the computational complexity of the SALONS in MATLAB flops is compared with that of some existing SOS-based localization methods for the NF sources such as the RD-MUSIC [48] and the GEMM [45]. Obviously the SALONS is computationally more efficient than these existing methods [48], [45], since the computationally burdensome eigendecomposition procedure and peak searching are avoided. □

IV. SOURCES TRACKING ALGORITHM

Based on the batch SALONS described above, now we consider the on-line algorithm for tracking the time-varying DOAs and ranges of multiple moving NF sources with crossover points on their trajectories.

Here we assume that $(\theta_k(n), r_k(n))$ are slowly time-varying so that $\theta_k(\bar{n}N_s + 1) \approx \theta_k(\bar{n}N_s + 2) \approx \cdots \approx \theta_k((\bar{n} + 1)N_s)$ and $r_k(\bar{n}N_s + 1) \approx r_k(\bar{n}N_s + 2) \approx \cdots \approx r_k((\bar{n} + 1)N_s)$ for
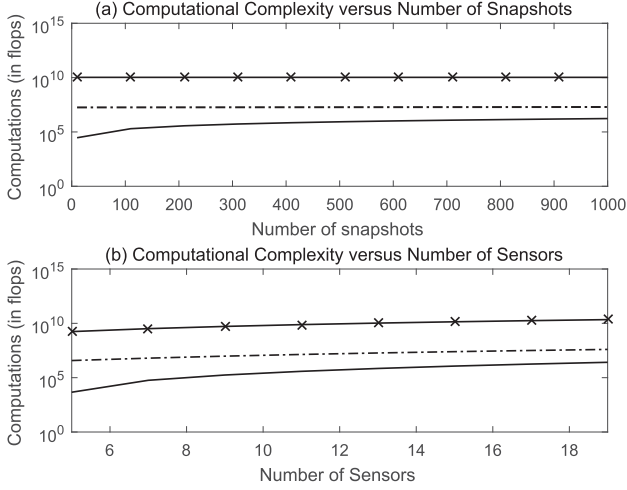
Fig. 2. Comparison of computational complexities in MATLAB flops versus (a) the number of the snapshots ($2M + 1 = 13$) and (b) the number of the sensors ($N = 200$) (solid line with "x": RD-MUSIC; dash-dotted line: GEMM; solid line: SALONS).

$n \in (\bar{n}N_s, (\bar{n} + 1)N_s]$ and $\bar{n} = 0, 1, \ldots$, where there are N_s snapshots of array data available for DOA updating (cf. [64]–[66] and references therein). Then by denoting $\theta_k(\bar{n}N_s)$ and $r_k(\bar{n}N_s)$ as $\theta_k(\bar{n})$ and $r_k(\bar{n})$, the DOA and range tracking can be formulated as the estimation of the location pairs $\{(\theta_k(\bar{n}), r_k(\bar{n}))\}$ from N_s snapshots of $\{\boldsymbol{x}(n)\}$ measured at $n = \bar{n}N_s + 1, \bar{n}N_s + 2, \ldots, (\bar{n} + 1)N_s$ while maintaining the correct association between the current estimates $(\hat{\theta}_k(\bar{n}), \hat{r}_k(\bar{n}))$ and the previous estimates $(\hat{\theta}_k(\bar{n} - 1), \hat{r}_k(\bar{n} - 1))$ for the same incident signal.

A. Luenberger Observer Based State Estimation

Similarly to the previously proposed FF sources tracking [65], [66], where the Luenberger observer [67] with a deterministic dynamic state model of the direction trajectory was employed to solve the association problem of the estimated DOAs at two successive time instants, here we consider the problem of multiple NF sources tracking by using the Luenberger observer. By letting the DOA (or range) velocity and acceleration of $\theta_k(\bar{n})$ (or $r_k(\bar{n})$) at the instant $\bar{n}$ be $\dot{\theta}_k(\bar{n})$ (or $\dot{r}_k(n)$) and $\ddot{\theta}_k(\bar{n})$ (or $\ddot{r}_k(\bar{n})$) and denoting the state vectors of the dynamic models for the DOA and range as $\boldsymbol{\zeta}_{\theta_k}(\bar{n}) \triangleq [\theta_k(\bar{n}), \dot{\theta}_k(\bar{n}), \ddot{\theta}_k(\bar{n})]^T$ and $\boldsymbol{\zeta}_{r_k}(\bar{n}) \triangleq [r_k(\bar{n}), \dot{r}_k(\bar{n}), \ddot{r}_k(\bar{n})]^T$, the slowly time-varying trajectories of angle $\theta_k(\bar{n})$ and range $r_k(\bar{n})$ can be approximately expressed by a deterministic state model with constant acceleration in the absence of process and measurement noises and the DOAs and ranges can be measured from the corresponding state vectors

$$\boldsymbol{\zeta}_{\theta_k}(\bar{n}) = \boldsymbol{F}\boldsymbol{\zeta}_{\theta_k}(\bar{n} - 1), \quad \theta_k(\bar{n}) = \boldsymbol{c}^T\boldsymbol{\zeta}_{\theta_k}(\bar{n}) \tag{27}$$

$$\boldsymbol{\zeta}_{r_k}(\bar{n}) = \boldsymbol{F}\boldsymbol{\zeta}_{r_k}(\bar{n} - 1), \quad r_k(\bar{n}) = \boldsymbol{c}^T\boldsymbol{\zeta}_{r_k}(\bar{n}) \tag{28}$$

where $\boldsymbol{F}$ and $\boldsymbol{c}$ are the transition matrix and the measurement vector given by $\boldsymbol{F} \triangleq [1, N_s, 0.5N_s^2; 0, 1, N_s; 0, 0, 1]$ and $\boldsymbol{c} \triangleq [1, 0, 0]^T$ (see, e.g., [64]–[66], [68], [97]).

Then by using the measurements $\theta_k(\bar{n})$ and $r_k(\bar{n})$, the Luenberger observers for estimation of the DOA and range at the instant $\bar{n}$ are given by (cf. [69] and references therein)

$$\hat{\boldsymbol{\zeta}}_{\theta_k}(\bar{n} + 1) = \bar{\boldsymbol{\zeta}}_{\theta_k}(\bar{n}) + \boldsymbol{g}_{\theta_k}(\theta_k(\bar{n}) - \boldsymbol{c}^T\hat{\boldsymbol{\zeta}}_{\theta_k}(\bar{n})) \tag{29}$$

$$\bar{\boldsymbol{\zeta}}_{\theta_k}(\bar{n}) = \boldsymbol{F}\hat{\boldsymbol{\zeta}}_{\theta_k}(\bar{n} - 1) \tag{30}$$

$$\hat{\theta}_k(\bar{n}) = \boldsymbol{c}^T\hat{\boldsymbol{\zeta}}_{\theta_k}(\bar{n}) \tag{31}$$

$$\hat{\boldsymbol{\zeta}}_{r_k}(\bar{n} + 1) = \bar{\boldsymbol{\zeta}}_{r_k}(\bar{n}) + \boldsymbol{g}_{r_k}(r_k(\bar{n}) - \boldsymbol{c}^T\hat{\boldsymbol{\zeta}}_{r_k}(\bar{n})) \tag{32}$$

$$\bar{\boldsymbol{\zeta}}_{r_k}(\bar{n}) = \boldsymbol{F}\hat{\boldsymbol{\zeta}}_{r_k}(\bar{n} - 1) \tag{33}$$

$$\hat{r}_k(\bar{n}) = \boldsymbol{c}^T\hat{\boldsymbol{\zeta}}_{r_k}(\bar{n}) \tag{34}$$

where $\hat{\boldsymbol{\zeta}}_{\theta_k}(\bar{n})$ (or $\hat{\boldsymbol{\zeta}}_{r_k}(\bar{n})$) is the current estimate based on the measurement $\theta_k(\bar{n})$ (or $r_k(\bar{n})$) at the current instant $\bar{n}$, while $\bar{\boldsymbol{\zeta}}_{\theta_k}(\bar{n})$ (or $\bar{\boldsymbol{\zeta}}_{r_k}(\bar{n})$) is the predicted estimate based on a model prediction from the estimate obtained at the previous instant $\bar{n} - 1$, and $\boldsymbol{g}_{\theta_k}$ and $\boldsymbol{g}_{r_k}$ are the observer gains, which should be chosen appropriately to ensure the magnitudes of all eigenvalues of the matrices $\boldsymbol{F} - \boldsymbol{g}_{\theta_k}\boldsymbol{c}^T\boldsymbol{F}$ and $\boldsymbol{F} - \boldsymbol{g}_{r_k}\boldsymbol{c}^T\boldsymbol{F}$ be strictly less than one so that the observers in (29)–(34) are asymptotically stable for any initial values of $\hat{\boldsymbol{\zeta}}_{\theta_k}(0)$ and $\hat{\boldsymbol{\zeta}}_{r_k}(0)$.

B. DOA and Range Tracking of Moving Sources

In fact, the measurements $\theta_k(\bar{n})$ and $r_k(\bar{n})$ and the state vectors $\hat{\boldsymbol{\zeta}}_{\theta_k}(\bar{n})$ and $\hat{\boldsymbol{\zeta}}_{r_k}(\bar{n})$ in (29) and (32) are unknown and should be estimated from the available array data by exploiting the batch SALONS and the Luenberger observer described above. During the interval of direction updating $(\bar{n}T, (\bar{n} + 1)T)$ (i.e., $n = \bar{n}N_s + 1, \bar{n}N_s + 2, \ldots, (\bar{n} + 1)N_s)$, the instantaneous estimated cross-correlation matrix $\hat{\boldsymbol{R}}$ in (19) can be recursively computed by rank-1 updating as

$$\hat{\boldsymbol{R}}(n) = \bar{\gamma}\hat{\boldsymbol{R}}(n - 1) + \boldsymbol{x}(n)\boldsymbol{x}^H(n) \tag{35}$$

where $\bar{\gamma}$ is the forgetting factor given by $0 < \bar{\gamma} < 1$, which should be selected appropriately to accommodate for the time-variations of DOAs and ranges and usually chosen close to one for achieving good tracking performance and reducing the sensitivity to additive noise. When $n = (\bar{n} + 1)N_s$, by forming the instantaneous estimates $\boldsymbol{Z}_0(n)$ in (13), from (35), we can obtain the instantaneous orthogonal projector $\boldsymbol{\Pi}_{\hat{Q}_0}(n)$ with (21) and (22), which is denoted as $\boldsymbol{\Pi}_{\hat{Q}_0}(\bar{n})$. Then by considering the Taylor series expansion of $f_0(\theta)$ in (23) and using the instantaneous orthogonal projector $\boldsymbol{\Pi}_{\hat{Q}_0}(n)$ and a predicated state vectors $\hat{\boldsymbol{\zeta}}_{\theta_k}(\bar{n}|\bar{n} - 1)$ (i.e., $\hat{\theta}_k(\bar{n}|\bar{n} - 1)$), the "measurement" $\tilde{\theta}_k(\bar{n})$ of the DOA $\theta_k(\bar{n})$ in (29) can be estimated with the approximate Newton iteration as

$$\tilde{\theta}_k(\bar{n}) = \hat{\theta}_k(\bar{n}|\bar{n} - 1) - \frac{\text{Re}\{\boldsymbol{d}_0^H(\theta)\boldsymbol{\Pi}_{\hat{Q}_0}(\bar{n})\boldsymbol{a}_0(\theta)\}}{\boldsymbol{d}_0^H(\theta)\boldsymbol{\Pi}_{\hat{Q}_0}(\bar{n})\boldsymbol{d}_0(\theta)}\Bigg|_{\theta = \hat{\theta}_k(\bar{n}|\bar{n} - 1)} \tag{36}$$

where $\boldsymbol{d}_0(\theta) \triangleq d(\boldsymbol{a}_0(\theta))/d\theta$, while the state vector $\hat{\boldsymbol{\zeta}}_{\theta_k}(\bar{n})$ in (29) can be estimated by refining the predicated state vector

$\hat{\boldsymbol{\zeta}}_{\theta_k}(\bar{n}|\bar{n} - 1)$ as

$$\hat{\boldsymbol{\zeta}}_{\theta_k}(\bar{n}|\bar{n}) = \hat{\boldsymbol{\zeta}}_{\theta_k}(\bar{n}|\bar{n} - 1) + \boldsymbol{g}_{\theta_k}(\tilde{\theta}_k(\bar{n}) - \hat{\theta}_k(\bar{n}|\bar{n} - 1)) \quad (37)$$

and hence the DOA $\theta_k(\bar{n})$ can be estimated as

$$\hat{\theta}_k(\bar{n}) = \boldsymbol{c}^T \hat{\boldsymbol{\zeta}}_{\theta_k}(\bar{n}|\bar{n}). \quad (38)$$

Here for improving the tracking performance of the NF ranges, we construct the instantaneous orthogonal projector for the range by using the full array data (see [70] in details). In a similar way, by using the instantaneous orthogonal projector $\boldsymbol{\Pi}_{\hat{Q}}(\bar{n})$ and a predicated state vector $\hat{\boldsymbol{\zeta}}_{r_k}(\bar{n}|\bar{n} - 1)$ (i.e., $\hat{r}_k(\bar{n}|\bar{n} - 1)$) and using the estimate $\hat{\theta}_k(\bar{n})$ in (38), we can obtain the "measurement" $\tilde{r}_k(\bar{n})$ of the range $r_k(\bar{n})$ in (32) by the following approximate Newton iteration

$$\tilde{r}_k(\bar{n}) = \hat{r}_k(\bar{n}|\bar{n} - 1)$$
$$- \frac{\text{Re}\{\boldsymbol{d}(\hat{\theta}_k(\bar{n}), r)\boldsymbol{\Pi}_{\hat{Q}}(\bar{n})\boldsymbol{a}(\hat{\theta}_k(\bar{n}), r)\}}{\boldsymbol{d}(\hat{\theta}_k(\bar{n}), r)\boldsymbol{\Pi}_{\hat{Q}}(\bar{n})\boldsymbol{d}(\hat{\theta}_k(\bar{n}), r)}\Bigg|_{r = \hat{r}_k(\bar{n}|\bar{n} - 1)}$$
$$(39)$$

where $\boldsymbol{d}(\theta, r) \triangleq d(\boldsymbol{a}(\theta, r))/dr$ and the calculation details of $\boldsymbol{\Pi}_{\hat{Q}}(\bar{n})$ can be found in [70]. Then by using this "measurement" in (39), we can get the state vector $\hat{\boldsymbol{\zeta}}_{r_k}(\bar{n})$ in (32) by refining the predicated state vector $\hat{\boldsymbol{\zeta}}_{r_k}(\bar{n}|\bar{n} - 1)$ as

$$\hat{\boldsymbol{\zeta}}_{r_k}(\bar{n}|\bar{n}) = \hat{\boldsymbol{\zeta}}_{r_k}(\bar{n}|\bar{n} - 1) + \boldsymbol{g}_{r_k}(\tilde{r}_k(\bar{n}) - \hat{r}_k(\bar{n}|\bar{n} - 1)) \quad (40)$$

and thus the range $r_k(\bar{n})$ can be estimated as

$$\hat{r}_k(\bar{n}) = \boldsymbol{c}^T \hat{\boldsymbol{\zeta}}_{r_k}(\bar{n}|\bar{n}). \quad (41)$$

C. On-Line Algorithm for Source Tracking

Hence we have the following on-line algorithm for tracking the DOAs and ranges of multiple moving NF sources.

1) Estimate the initial values of $\theta_k(\bar{n})$ and $r_k(\bar{n})$ from the N_s snapshots of $\{\boldsymbol{x}(n)\}_{n=1}^{N_s}$ with the batch SALONS method described in Section III-C, and denote them as $\hat{\theta}_k(0|0)$ and $\hat{r}_k(0|0)$.

2) Initialize the Luenberger observers by $\hat{\boldsymbol{\zeta}}_{\theta_k}(0|0) = [\hat{\theta}_k(0|0), 0, 0]^T$ and $\hat{\boldsymbol{\zeta}}_{r_k}(0|0) = [\hat{r}_k(0|0), 0, 0]^T$, and set the instantaneous covariance matrix $\hat{\boldsymbol{R}}(N_s) = \boldsymbol{O}_{(2M+)\times(2M+1)}$, while update the instant index to $\bar{n} = 1$ and $n = \bar{n}N_s + 1$.

3) Calculate the predicted state vectors $\hat{\boldsymbol{\zeta}}_{\theta_k}(\bar{n}|\bar{n} - 1)$ and $\hat{\boldsymbol{\zeta}}_{r_k}(\bar{n}|\bar{n} - 1)$ and predicted angle $\hat{\theta}_k(\bar{n}|\bar{n} - 1)$ and range $\hat{r}_k(\bar{n}|\bar{n} - 1)$ from the existing estimated state vectors $\hat{\boldsymbol{\zeta}}_{\theta_k}(\bar{n} - 1|\bar{n} - 1)$ and $\hat{\boldsymbol{\zeta}}_{r_k}(\bar{n} - 1|\bar{n} - 1)$ with Luenberger observers with (30), (31), (33) and (34) as

$$\hat{\boldsymbol{\zeta}}_{\theta_k}(\bar{n}|\bar{n} - 1) = \boldsymbol{F}\hat{\boldsymbol{\zeta}}_{\theta_k}(\bar{n} - 1|\bar{n} - 1) \quad (42)$$

$$\hat{\boldsymbol{\zeta}}_{r_k}(\bar{n}|\bar{n} - 1) = \boldsymbol{F}\hat{\boldsymbol{\zeta}}_{r_k}(\bar{n} - 1|\bar{n} - 1) \quad (43)$$

$$\hat{\theta}_k(\bar{n}|\bar{n} - 1) = \boldsymbol{c}^T \hat{\boldsymbol{\zeta}}_{\theta_k}(\bar{n}|\bar{n} - 1) \quad (44)$$

$$\hat{r}_k(\bar{n}|\bar{n} - 1) = \boldsymbol{c}^T \hat{\boldsymbol{\zeta}}_{r_k}(\bar{n}|\bar{n} - 1). \quad (45)$$

4) Estimate the instantaneous cross-correlation matrix $\hat{\boldsymbol{R}}(n)$ with (35).

5) If $n = (\bar{n} + 1)N_s$, go to the next step; otherwise update the instant index as $n = n + 1$, and return to Step 4.

6) Calculate the estimated orthogonal projector $\boldsymbol{\Pi}_{\hat{Q}_0}(\bar{n})$ with (21) and (22).

7) Calculate the "measurement" $\tilde{\theta}_k(\bar{n})$ by using the projector $\boldsymbol{\Pi}_{\hat{Q}_0}(\bar{n})$ and the predicted angle $\hat{\theta}_k(\bar{n}|\bar{n} - 1)$ with (36), and estimate the DOAs $\hat{\theta}_k(\bar{n})$ with (37) and (38) for $k = 1, 2, \ldots, p$.

8) Calculate the estimated orthogonal projector $\boldsymbol{\Pi}_{\hat{Q}}(\bar{n})$ in (39) by using $\hat{\theta}_k(\bar{n})$, and estimate the "measurement" $\tilde{r}_k(\bar{n})$ by using the predicted angle $\hat{r}_k(\bar{n}|\bar{n} - 1)$ with (39).

9) Calculate the refined state vector $\hat{\boldsymbol{\zeta}}_{r_k}(\bar{n}|\bar{n})$ and estimate the range $\hat{r}_k(\bar{n})$ with (40) and (41).

10) Update the instant index of angle and range updating as $\bar{n} = \bar{n} + 1$ and $n = \bar{n}N_s + 1$, and go to Step 3.

Remark E: The Luenberger observer plays important roles of refining (or smoothing) the measured DOA and range $\tilde{\theta}_k(\bar{n})$ and $\tilde{r}_k(\bar{n})$ obtained from the array data and maintaining the association between the estimates $\{(\hat{\theta}_k(\bar{n}), \hat{r}_k(\bar{n}))\}$ at different time instants of parameter updating.   □

V. STATISTICAL ANALYSIS OF BATCH SALONS

Here we analyze the statistical properties of the batch SA-LONS for NF source localization with (23) and (24) for a large number of snapshots.

A. Asymptotic Properties of the Proposed Method

For sufficiently larger number of snapshots N, we can find that the estimated DOA $\hat{\theta}_k$ by minimizing the cost function in (23) and the estimated range $\hat{r}_k$ by minimizing the cost function in (24) approach the true parameters θ_k and r_k with probability one (cf. Appendix A in [59]). Hence we can obtain the asymptotic MSE expressions of the DOAs and ranges estimated by the SALONS as the following Theorems.

Theorem 1: The large-sample MSE of the estimation error $\hat{\theta}_k - \theta_k$ of the near-field signals obtained by (23) is given by

$$\text{MSE}(\hat{\theta}_k) = \text{var}\{\hat{\theta}_k\}$$
$$= \frac{\sigma^2}{2NH_{0kk}^2}\text{Re}\{\sigma^2 \text{Tr}\{\boldsymbol{M}_{0k}\boldsymbol{M}_{0k}\} + \sigma^2 \text{Tr}\{\boldsymbol{M}_{0k}\boldsymbol{M}_{0k}^H\}$$
$$+ 2\text{Tr}\{\boldsymbol{M}_{0k}\bar{\boldsymbol{R}}\boldsymbol{M}_{0k}\} + \text{Tr}\{\boldsymbol{M}_{0k}^H\bar{\boldsymbol{R}}\boldsymbol{M}_{0k}\}$$
$$+ \text{Tr}\{\boldsymbol{M}_{0k}\bar{\boldsymbol{R}}\boldsymbol{M}_{0k}^H\}\} \quad (46)$$

where $\boldsymbol{g}_0(\theta_k) \triangleq \boldsymbol{\Pi}_{Q_0}\boldsymbol{d}_0(\theta_k)$, $\boldsymbol{h}_0(\theta_k) \triangleq \boldsymbol{Z}_{01}^H(\boldsymbol{Z}_{01}\boldsymbol{Z}_{01}^H)^{-1}$ $\cdot\boldsymbol{a}_{01}(\theta_k)$, $H_{0kk} \triangleq \boldsymbol{d}_0^H(\theta_k)\boldsymbol{\Pi}_{Q_0}\boldsymbol{d}_0(\theta_k)$, $\boldsymbol{d}_0(\theta_k) \triangleq d\boldsymbol{a}_0(\theta)/(d\theta)|_{\theta=\theta_k}$, $\boldsymbol{M}_{0k} \triangleq (\boldsymbol{g}_0^H(\theta_k) \otimes \boldsymbol{I}_{2M+1})\boldsymbol{C}_0(\boldsymbol{h}_0(\theta_k) \otimes \boldsymbol{I}_{2M+1})$, $\bar{\boldsymbol{R}} = \boldsymbol{R} - \sigma^2\boldsymbol{I}_{2M+1}$, $\boldsymbol{a}_{01}(\theta_k)$ denotes the k column of $\tilde{\boldsymbol{A}}_{01}^*$, and $\boldsymbol{C}_0 = \boldsymbol{C}_m|_{m=0}$ given in (47) at the bottom of the next page.

Proof: See Appendix A.   ∎

Theorem 2: The large-sample MSE of the estimation error $\hat{r}_k - r_k$ of the near-field signals obtained by (24) is given by

$$
\begin{aligned}
\mathrm{MSE}(\hat{r}_k) &= \mathrm{var}\{\hat{r}_k\} \\
&= \frac{\bar{H}_{\bar{m}kk}^2}{H_{\bar{m}kk}^2}\mathrm{MSE}(\hat{\theta}_k) \\
&\quad + \frac{\sigma^2}{2NH_{\bar{m}kk}^2}\mathrm{Re}\{\sigma^2\mathrm{Tr}\{\boldsymbol{M}_{\bar{m}k}\boldsymbol{M}_{\bar{m}k}\} \\
&\quad + \sigma^2\mathrm{Tr}\{\boldsymbol{M}_{\bar{m}k}\boldsymbol{M}_{\bar{m}k}^H\} + 2\mathrm{Tr}\{\boldsymbol{M}_{\bar{m}k}\bar{\boldsymbol{R}}\boldsymbol{M}_{\bar{m}k}\} \\
&\quad + \mathrm{Tr}\{\boldsymbol{M}_{\bar{m}k}^H\bar{\boldsymbol{R}}\boldsymbol{M}_{\bar{m}k}\} + \mathrm{Tr}\{\boldsymbol{M}_{\bar{m}k}\bar{\boldsymbol{R}}\boldsymbol{M}_{\bar{m}k}^H\}\} \\
&\quad + \frac{\sigma^2\bar{H}_{\bar{m}kk}}{NH_{\bar{m}kk}^2 H_{0kk}}\mathrm{Re}\{\sigma^2\mathrm{Tr}\{\boldsymbol{M}_{\bar{m}k}\boldsymbol{M}_{0k}\} \\
&\quad + \sigma^2\mathrm{Tr}\{\boldsymbol{M}_{\bar{m}k}\boldsymbol{M}_{0k}^H\} + 2\mathrm{Tr}\{\boldsymbol{M}_{\bar{m}k}\bar{\boldsymbol{R}}\boldsymbol{M}_{0k}\} \\
&\quad + \mathrm{Tr}\{\boldsymbol{M}_{\bar{m}k}^H\bar{\boldsymbol{R}}\boldsymbol{M}_{0k}\} + \mathrm{Tr}\{\boldsymbol{M}_{\bar{m}k}\bar{\boldsymbol{R}}\boldsymbol{M}_{0k}^H\}\}
\end{aligned}
\tag{48}
$$

where $\boldsymbol{g}_{\bar{m}}(\theta_k, r_k) \triangleq \boldsymbol{\Pi}_{Q_{\bar{m}}} \boldsymbol{d}_{\bar{m}}(\theta_k, r_k)$, $\boldsymbol{h}_{\bar{m}}(\theta_k, r_k) \triangleq \boldsymbol{Z}_{\bar{m}1}^H (\boldsymbol{Z}_{\bar{m}1}\boldsymbol{Z}_{\bar{m}1}^H)^{-1}\boldsymbol{a}_{\bar{m}1}(\theta_k, r_k)$, $H_{\bar{m}kk} \triangleq \boldsymbol{d}_{\bar{m}r}^H(\theta_k, r_k)\boldsymbol{\Pi}_{Q_{\bar{m}}} \boldsymbol{d}_{\bar{m}r}(\theta_k, r_k)$, $\bar{H}_{\bar{m}kk} \triangleq -\boldsymbol{d}_{\bar{m}r}^H(\theta_k, r_k)\boldsymbol{\Pi}_{Q_{\bar{m}}} \boldsymbol{d}_{\bar{m}\theta}(\theta_k, r_k)$, $\boldsymbol{d}_{\bar{m}r}(\theta_k, r_k) \triangleq \partial\boldsymbol{a}_{\bar{m}}(\theta_k, r_k)/(\partial r)|_{r=r_k}$, $\boldsymbol{d}_{\bar{m}\theta}(\theta_k, r_k) \triangleq \partial\boldsymbol{a}_{\bar{m}}(\theta_k, r_k)/(\partial\theta)|_{\theta=\theta_k}$, $\boldsymbol{M}_{\bar{m}k} \triangleq (\boldsymbol{g}_{\bar{m}}^H(\theta_k, r_k) \otimes \boldsymbol{I}_{2M+1}) \cdot \boldsymbol{C}_{\bar{m}}(\boldsymbol{h}_{\bar{m}}(\theta_k, r_k) \otimes \boldsymbol{I}_{2M+1})$, $\boldsymbol{a}_{\bar{m}1}(\theta_k)$ denotes the k column of $\tilde{\boldsymbol{A}}_{\bar{m}1}^*$, and $\boldsymbol{C}_{\bar{m}} = \boldsymbol{C}_m|_{m=\bar{m}}$ given in (47) at the bottom of this page.

Proof: See Appendix B. ∎

B. An Analytic Study of Performance

As the general expressions of asymptotic MSEs derived in above are much complicated, here we specialize in the case of one source signal $s_1(n)$ impinging from (θ_1, r_1) for gaining insights into the SALONS for source localization.

In this case (i.e., $K = 1$), by letting $m = 0$, we readily obtain

$$
L = \bar{K} = M + 1
\tag{49}
$$

$$
\tilde{\boldsymbol{A}}_0^* = \left[1, e^{-2j\gamma_{01}}, \dots, e^{-j2M\gamma_{01}}\right]^T \triangleq \boldsymbol{a}_0^*
\tag{50}
$$

$$
\bar{\boldsymbol{A}}_0^T = \left[1, e^{2j\gamma_{01}}, \dots, e^{j2M\gamma_{01}}\right] \triangleq \boldsymbol{a}_0^T
\tag{51}
$$

$$
\boldsymbol{d}_0(\theta_1) = j\psi\left[0, e^{-2j\gamma_{01}}, \dots, Me^{-2j\gamma_{01}}\right]^T \triangleq \boldsymbol{d}_0
\tag{52}
$$

$$
\bar{\boldsymbol{R}}_{0s} = r_{s1}
\tag{53}
$$

$$
\boldsymbol{D}_0 = e^{j2\gamma_{01}}
\tag{54}
$$

$$
\gamma_{01} = \psi_1 = -\frac{2\pi d}{\lambda}\sin\theta_1
\tag{55}
$$

and $a_{01}(\theta_1) = 1$, where $\psi \triangleq (4\pi d/\lambda)\cos\theta_1$. Then we can obtain

$$
\boldsymbol{a}_0^H \boldsymbol{a}_0 = M + 1
\tag{56}
$$

$$
\boldsymbol{d}_0^H \boldsymbol{a}_0 = -j\psi\frac{M(M+1)}{2}
\tag{57}
$$

$$
\boldsymbol{d}^H \boldsymbol{d}_0 = \psi^2\frac{M(M+1)(2M+1)}{6}
\tag{58}
$$

$$
\begin{aligned}
H_{011} &= \boldsymbol{d}_0^H \boldsymbol{\Pi}_{Q_0} \boldsymbol{d}_0 = \boldsymbol{d}_0^H \left(\boldsymbol{I}_{M+1} - \boldsymbol{a}_0^* (\boldsymbol{a}_0^T \boldsymbol{a}_0^*)^{-1} \boldsymbol{a}_0^T\right) \boldsymbol{d}_0 \\
&= \psi^2\frac{M(M+1)(M+2)}{12}
\end{aligned}
\tag{59}
$$

$$
\boldsymbol{g}_0(\theta_1) = \boldsymbol{\Pi}_{Q_0} \boldsymbol{d}_0
\tag{60}
$$

$$
\boldsymbol{h}_0(\theta_1) = \boldsymbol{Z}_{01}^H \left(\boldsymbol{Z}_{01}\boldsymbol{Z}_{01}^H\right)^{-1} a_{01}(\theta_1) = \frac{\boldsymbol{a}_0^*}{r_{s1}(M+1)}.
\tag{61}
$$

Therefore by substituting those results into (46) and by performing some calculations, from Theorem 1, we can obtain the asymptotic MSE of the estimated DOA of the NF signal as

$$
\mathrm{MSE}(\hat{\theta}_1) = \frac{1}{\psi^2 N}\frac{6}{\mathrm{SNR}}\frac{1}{M(M+1)^3(M+2)}\left(\alpha + \frac{\beta}{\mathrm{SNR}}\right)
\tag{62}
$$

where

$$
\alpha \triangleq 2\boldsymbol{a}_0^H \boldsymbol{F}\boldsymbol{F}\boldsymbol{a}_0 + \boldsymbol{a}_0^H \boldsymbol{F}\boldsymbol{F}^H \boldsymbol{a}_0 + \boldsymbol{a}_0^H \boldsymbol{F}^H \boldsymbol{F}\boldsymbol{a}_0
\tag{63}
$$

$$
\beta \triangleq -\mathrm{Tr}\{\boldsymbol{F}\boldsymbol{F}\} - \mathrm{Tr}\{\boldsymbol{F}^H \boldsymbol{F}\}
\tag{64}
$$

$$
\boldsymbol{F} \triangleq (\boldsymbol{g}_0^H(\theta_1) \otimes \boldsymbol{I}_{2M+1})\boldsymbol{C}_0(\boldsymbol{a}_0^* \otimes \boldsymbol{I}_{2M+1})
\tag{65}
$$

and we set $\mathrm{SNR} = r_{s1}/\sigma^2$. Hence from (62), we can find that the asymptotic MSE $\mathrm{MSE}(\hat{\theta}_1)$ of the estimated DOA $\hat{\theta}_1$ decreases monotonically with increasing the number of snapshots N or SNR, which means that the SALONS estimator is asymptotically efficient for sufficiently large number of snapshots N.

Unfortunately, the analytic study of the asymptotic MSE $\mathrm{MSE}(\hat{r}_1)$ of the estimated range r_1 is much more complicated and rather tedious to obtain herein, while the empirical examinations in Section VI show that the asymptotic MSE of the estimated range also decreases monotonically with the increasing N or SNR.

VI. NUMERICAL EXAMPLES

In this section, we evaluate the estimation performance and the statistical property of the batch SALONS and the tracking performance of the proposed adaptive algorithm through numerical examples. A ULA consisting of $2M + 1 = 11$ (i.e., $M = 5$) sensors is used, where the sensor spacing $d = \lambda/4$, and the SNR is defined as the ratio of the signal power to the noise

$$
\boldsymbol{C}_m = \begin{bmatrix} \boldsymbol{e}_{2M+2-\bar{K}-m_1}\boldsymbol{e}_{\bar{K}+m_2}^T, & \boldsymbol{e}_{2M+3-\bar{K}-m_1}\boldsymbol{e}_{\bar{K}-1+m_2}^T, & \cdots, & \boldsymbol{e}_{2M+1-m_1}\boldsymbol{e}_{1+m_2}^T \\ \boldsymbol{e}_{2M+1-\bar{K}-m_1}\boldsymbol{e}_{\bar{K}+1+m_2}^T, & \boldsymbol{e}_{2M+2-\bar{K}-m_1}\boldsymbol{e}_{\bar{K}+m_2}^T, & \cdots, & \boldsymbol{e}_{2M-m_1}\boldsymbol{e}_{2+m_2}^T \\ \vdots & \vdots & \ddots & \vdots \\ \boldsymbol{e}_{1-m_1}\boldsymbol{e}_{2M+1+m_2}^T, & \boldsymbol{e}_{2-m_1}\boldsymbol{e}_{2M+m_2}^T, & \cdots, & \boldsymbol{e}_{\bar{K}-m_1}\boldsymbol{e}_{2M+2+m_2}^T \end{bmatrix}
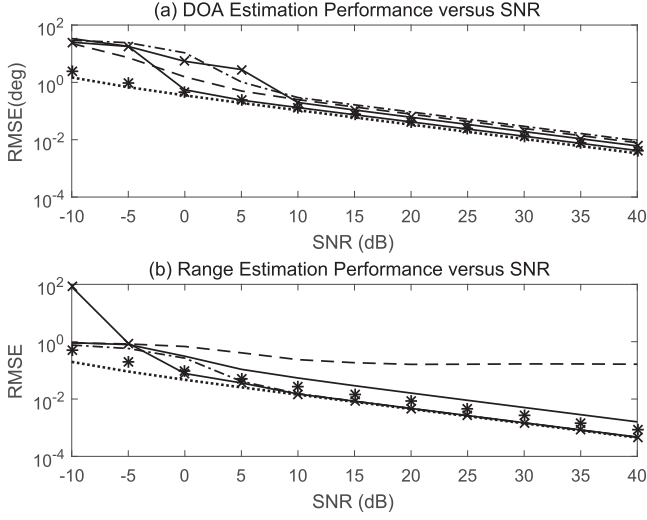\tag{47}
$$

Fig. 3.   RMSEs of the (a) DOA and (b) range estimates versus the SNR (dashed line: WLPM; dash-dotted line: GEMM; solid line with "x": RD-MUSIC; solid line: SALONS; "∗": theoretical RMSE; dotted line: CRB) for Example 1 ($N = 128$, $(2°, 2.9λ)$, and $(19°, 3.3λ)$).
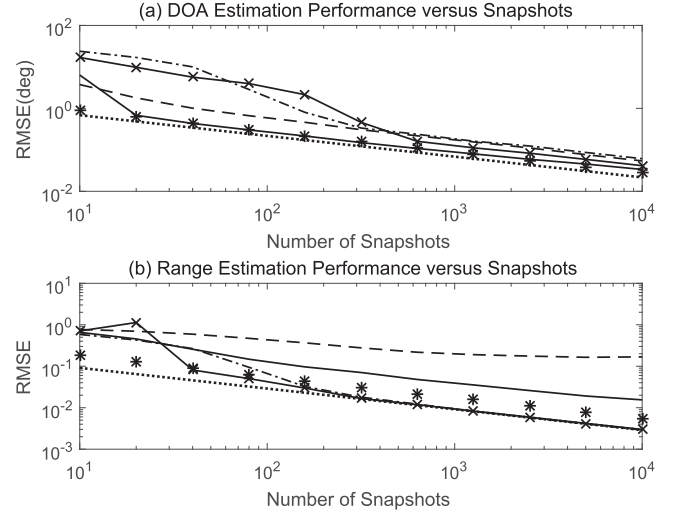

Fig. 4.   RMSEs of the (a) DOA and (b) range estimates versus the number of snapshots (dashed line: WLPM; dash-dotted line: GEMM; solid line with "x": RD-MUSIC; solid line: SALONS; "∗": theoretical RMSE; dotted line: CRB) for Example 1 ($\text{SNR} = 5$ dB, $(2°, 2.9λ)$, and $(19°, 3.3λ)$).

variance at each sensor. In the simulations, the WLPM [44], the GEMM [45], the RD-MUSIC [48], and the stochastic CRB [44] are carried out for comparison of source localization. In order to measure the overall performance of estimating the DOA and range, we define the root MSEs (RMSEs) for the DOA and range of the kth incident signals $s_k(n)$, respectively

$$\text{RMSE}(\theta) = \sqrt{\frac{1}{K\bar{N}} \sum_{i=1}^{\bar{N}} \sum_{k=1}^{K} \left(\hat{\theta}_k^{(i)} - \theta_k\right)^2} \quad (66)$$

$$\text{RMSE}(r) = \sqrt{\frac{1}{K\bar{N}} \sum_{i=1}^{\bar{N}} \sum_{k=1}^{K} \frac{\left(\hat{r}_k^{(i)} - r_k\right)^2}{r_k^2}} \quad (67)$$

where $\hat{\theta}_k^{(i)}$ and $\hat{r}_k^{(i)}$ denote the estimates of θ_k and r_k at the ith trial, respectively. The results in each example below are obtained from $\bar{N} = 500$ independent trails, and $\bar{m}$ is set at $\bar{m} = 1$ for Examples 1 and 2.

Example 1 (Performance versus SNR): Firstly we examine the estimation performance of the presented SALONS with respect to the SNR. There are two NF sources with equal power (i.e., $r_{s_1} = r_{s_2} = r_s$) localized at $(2°, 2.9λ)$ and $(19°, 3.3λ)$, while the SNR is varied from -10 dB to 40 dB, and the number of snapshots is fixed at $N = 128$. The sources are noncoherent with the correlation matrix (e.g., [63]) as follows

$$\boldsymbol{R}_s = \frac{1}{\sigma^2} \begin{bmatrix} 10^{\frac{\text{SNR}_1}{10}} & 0 \\ 0 & 10^{\frac{\text{SNR}_2}{10}} \end{bmatrix} \quad (68)$$

where $\text{SNR}_1 = \text{SNR}_2 = r_s/\sigma^2$, and the signal power is kept equal to one for each simulation.

The averaged RMSEs of the estimated DOAs and ranges of two NF source signals in terms of the SNR are shown in Figs. 3(a) and 3(b), respectively. Obviously the DOA estimation performance of the presented SALONS performs better than the WLPM [44], the GEMM [45], and the RD-MUSIC [48], where the computationally burdensome eigendecomposi-

tion is also avoided in the proposed method, while the range estimation has a satisfactory performance, and the RMSEs decreased consistently with the increasing SNRs. However, the proposed method has a relatively higher RMSEs for the range estimation especially at high SNRs than the some existing methods such as the GEMM [45] and the RD-MUSIC [48]. This is due to the limited data (only the anti-diagonal elements of the covariance matrix) used for the estimation, while the proposed method still shows a better range estimation performance comparing to the similar method such as WLPM [44]. Further, the empirical RMSEs of the proposed method coincide well with the theoretical RMSEs derived in Section IV (except at low SNR), and they decrease monotonically with the increasing SNR and are very close to the CRB.

Example 2 (Performance versus Number of Snapshots): Then we test the performance of the presented SALONS in terms of the number of snapshots. The simulation conditions are similar to those in Example 1, except that the SNR is set at 5 dB, and the number of snapshots is varied from 10 to 10000.

The empirical RMSEs of the DOAs and ranges against the number of snapshots are plotted in Figs. 4(a) and 4(b), and they are compared with the WLPM [44], the GEMM [45], the RD-MUSIC [48], and the stochastic CRB [44]. The presented SALONS has better DOAs estimation performance than the WLPM, the GEMM, the RD-MUSIC. However, as mentioned above, the ranges estimation generally decreased with the increasing number of snapshots, while the RMSEs of the ranges estimation of the proposed method are higher than the GEMM and the RD-MUSIC due to the limited data we used. The empirical RMSEs of the estimated DOAs and that of the estimated ranges agree very well with the theoretical RMSEs derived in Section IV, and they are very close to the CRB when the number of snapshots becomes large.

Example 3 (Tracking Performance of On-Line Algorithm): Finally we assess the tacking performance of the proposed on-line algorithm for source tracking, where there are two
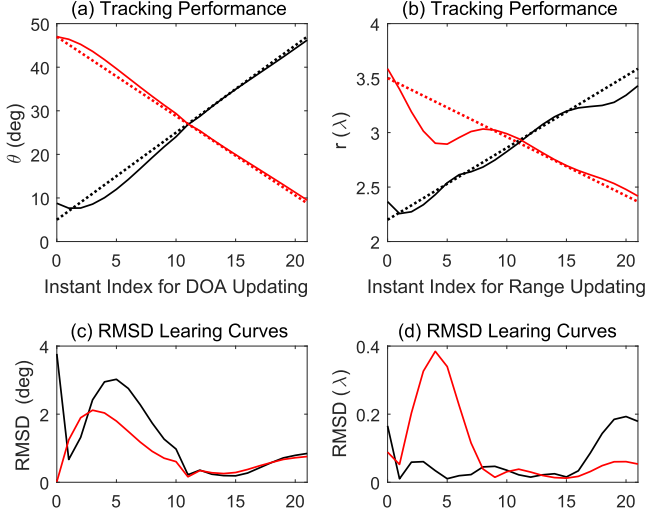
Fig. 5. Averaged estimates of (a) $\theta_k(\bar{n})$ and (b) $r_k(\bar{n})$ of two uncorrelated NF signals with crossings and RMSD learning curves of (c) $\mathrm{RMSD}(\hat{\theta}_k(\bar{n}))$ and $\mathrm{RMSD}(\hat{r}_k(\bar{n}))$ in Example 3 (dotted line: actual values; red solid lines: $\hat{\theta}_1(\bar{n})$ or $\hat{r}_1(\bar{n})$; and back solid lines: $\hat{\theta}_2(\bar{n})$ or $\hat{r}_2(\bar{n})$; SNR = 5 dB, $M = 4$, $N_s = 200$, and $\bar{\gamma} = 0.99$).

uncorrelated NF sources with the time varying DOAs and ranges $(\theta_1(n), r_1(n))$ and $(\theta_2(n), r_2(n))$ with SNR = 5 dB, where $(\theta_1(0), r_1(0)) = (47°, 3.5\lambda)$ and $(\theta_2(0), r_2(0)) = (5°, 2.2\lambda)$ as shown in Figs. 5 (a) and 5(b), and $N_s = 200$. The forgetting factor $\bar{\gamma}$ in (35) is set as $\bar{\gamma} = 0.99$, and the Luenberger observer gains $\{g_{\theta_k}\}$ and $\{g_{r_k}\}$ in (29) and (32) are chosen as $g_{\theta_1} = g_{r_1} = [0.5070, 0.1493/N_s, 0.0165/N_s^2]^T$ and $g_{\theta_2} = g_{r_2} = [0.5070, 0.1399/N_s, 0.0143/N_s^2]^T$, where the Luenberger observer gains are chosen by the technique used in [65] (see Appendix in [65] for details).

Here we define the empirical root mean-squared-derivation (RMSD) learning curves of the estimated DOA and range $\hat{\theta}_k(\bar{n})$ and $\hat{r}_k(\bar{n})$ as

$$\mathrm{RMSD}(\hat{\theta}_k(\bar{n})) \triangleq \sqrt{\frac{1}{\bar{N}} \sum_{i=1}^{\bar{N}} \left(\theta_k(\bar{n}) - \hat{\theta}_k^{(i)}(\bar{n}) \right)^2} \quad (69)$$

$$\mathrm{RMSD}(\hat{r}_k(\bar{n})) \triangleq \sqrt{\frac{1}{\bar{N}} \sum_{i=1}^{\bar{N}} \left(r_k(\bar{n}) - \hat{r}_k^{(i)}(\bar{n}) \right)^2} \quad (70)$$

where $\hat{\theta}_k^{(i)}(\bar{n})$ and $\hat{r}_k^{(i)}(\bar{n})$ are the estimates obtained in the ith trial at the instant $\bar{n}$. The trajectories of the actual DOAs and their averaged estimates $\{\hat{\theta}_k(\bar{n})\}$, and their empirical RMSD learning curves are plotted in Figs. 5(a) and 5(c), while the corresponding results for the ranges $\{r_k(\bar{n})\}$ are shown in Figs. 5(b) and 5(d), respectively. As described above, because the computationally expensive eigendecomposition process and pair-matching procedure are avoided, the SALONS method is feasible for the on-line implementation. Moreover due to the utilization of the Luenberger state observer, the presented on-line algorithm can achieve correct association of estimates $\hat{\theta}_k(\bar{n})$ and $\hat{r}_k(\bar{n})$ at two successive instants of direction updating. From the empirical mean and RMSD behaviors shown in Fig. 5, we can see that the proposed on-line algorithm has good capability for tracking the time-varying DOAs and ranges of multiple NF sources with crossings on their trajectories.

VII. CONCLUSION

In this paper, two subspace-based batch and adaptive algorithms were presented for localization and tracking of multiple NF sources by utilizing the advantages of a symmetric ULA and the SOS of array data, where the computationally burdensome eigendecomposition and spectrum peak searching are avoided, and the estimated DOAs and ranges are automatically paired without any additional processing. The statistical performance of the batch SALONS was analyzed, and the asymptotic MSE expressions of the estimated DOAs and ranges were derived explicitly. Finally, the effectiveness and the theoretical analysis were substantiated through numerical examples.

APPENDIX A
PROOF OF THEOREM 1

As studied in [59], [61], [62], [66], the first-order expression for the estimation error $\Delta\theta_k \triangleq \hat{\theta}_k - \theta_k$ of the NF signals can be obtained as

$$\Delta\theta_k \approx -\frac{f_0'(\theta_k)}{f_0''(\theta_k)} \approx -\frac{\mathrm{Re}\left\{ d_0^H(\theta)\Pi_{\hat{Q}_0} a_0(\theta) \right\}}{d_0^H(\theta)\Pi_{Q_0} d_0(\theta)} \quad (A1)$$

where a first-order approximation of the estimated orthogonal projector $\Pi_{\hat{Q}_0}$ in (A1) is given by [59], [61]

$$\Pi_{\hat{Q}_0} \approx (\hat{Q}_0 - Q_0)(Q_0^H Q_0)^{-1}Q_0^H + Q_0(Q_0^H Q_0)^{-1}$$
$$\cdot (\hat{Q}_0 - Q)_0^H + (Q_0^H \hat{Q}_0)^{-1}Q_0^H. \quad (A2)$$

By using the fact that $Q_0^H a_0(\theta_k) = 0_{(L-K)\times 1}$ and substituting (A2) into (A1), the estimation error $\Delta\theta_k$ can be approximated as

$$\Delta\theta_k \approx -\frac{\mathrm{Re}\left\{ d_0^H(\theta_k)Q_0(Q_0^H Q_0)^{-1}\hat{Q}_0^H a_0(\theta_k) \right\}}{d_0^H(\theta)\Pi_{Q_0} d_0(\theta)}$$
$$= -\frac{\mathrm{Re}\{\mu_k\}}{H_{0kk}} \quad (A3)$$

where

$$\mu_k \triangleq d_0^H(\theta_k)Q_0(Q_0^H Q_0)^{-1}\hat{Q}_0^H a_0(\theta_k)$$
$$= d_0^H(\theta_k)Q_0(Q_0^H Q_0)^{-1}\tilde{P}_0^H a_{01}(\theta_k) \quad (A4)$$

in which $a_{01}(\theta_k)$ denotes the k column of $\tilde{A}_{01}^*$ with $k = 1, 2, \ldots, K$, and

$$\tilde{P}_0^H \triangleq \hat{P}_0^H - P_0^H$$
$$= \left(\hat{Z}_{02}\hat{Z}_{01}^H - P_0^H \hat{Z}_{01}\hat{Z}_{01}^H \right)\left(\hat{Z}_{01}\hat{Z}_{01}^H \right)^{-1}$$
$$\approx -Q_0^H \hat{Z}_0 Z_{01}^H \left(Z_{01}Z_{01}^H \right)^{-1} \quad (A5)$$

where $Q_0^H Z_0 = O_{(L-K)\times(L)}$ is used. By substituting (A5) into (A4) and noting that $\hat{\tilde{R}} = \hat{R} - \hat{\sigma}^2 I_{2M+1}$, we have

$$\mu_k = -d_0^H(\theta_k)\Pi_{Q_0} \hat{Z}_0 Z_{01}^H (Z_{01}Z_{01}^H)^{-1}a_{01}(\theta_k)$$
$$= -g_0^H(\theta_k)\hat{Z}_0 h_0(\theta_k). \quad (A6)$$

By using the fact that

$$\hat{\bar{\rho}}_m(p) = \bar{e}_{M+p+1}^T(\hat{R} - \hat{\sigma}^2 I_{2M+1})\bar{e}_{M-p+1} \quad (\text{A7})$$

and from (13), we have

$$\hat{Z}_m = \frac{1}{N}\sum_{n=1}^{N}(I_L \otimes x^H(n))C_m(I_{\bar{K}} \otimes x(n)) - \hat{\sigma}^2 B_m \quad (\text{A8})$$

where B_m is given in (A9) at the bottom of this page, and we can easily see that $B_0 = I_{M+1}$. Then from (A6)–(A8), we have

$$\mu_k = -\frac{1}{N}\sum_{n=1}^{N} g_0^H(\theta_k)(I_{M+1} \otimes x^H(n))$$
$$\cdot C_0(I_{M+1} \otimes x(n))h_0(\theta_k)$$
$$= -\frac{1}{N}\sum_{n=1}^{N} x^H(n)(g_0^H(\theta_k) \otimes I_{2M+1})$$
$$\cdot C_0(h_0(\theta_k) \otimes I_{2M+1})x(n)$$
$$= -\frac{1}{N}\sum_{n=1}^{N} x^H(n)M_{0k}x(n) \quad (\text{A10})$$

where the facts that $Q_0^H Z_{01} = O_{(M+1-K)\times K}$ and $g_0^H(\theta_k) \cdot h_0(\theta_k) = 0$ are used implicitly.

Since the estimate $\hat{\theta}_k$ is consistent, from (A3), the MSE (or variance) of the estimation error $\Delta\theta_k$ is given by

$$\text{MSE}(\hat{\theta}_k) \triangleq E\{(\Delta\theta_k)^2\} = \text{var}(\hat{\theta}_k)$$
$$\approx \frac{1}{2H_{0kk}^2}\text{Re}\{E\{\mu_k^2\} + E\{|\mu_k|^2\}\} \quad (\text{A11})$$

where we use the fact that $\text{Re}\{\mu_i\}\text{Re}\{\mu_k\} = 0.5(\text{Re}\{\mu_i\mu_k\} + \text{Re}\{\mu_i\mu_k*\})$ implicitly. By substituting the relation $x(n) = \bar{x}(n) + w(n)$ (i.e., $\bar{x}(n) \triangleq As(n)$) into (A10), we can rewrite μ_k in (A10) as

$$\mu_k = -\frac{1}{N}\sum_{n=1}^{N}\left(\bar{x}^H(n)M_{0k}\bar{x}(n) + \bar{x}^H(n)M_{0k}w(n)\right.$$
$$\left. + w^H(n)M_{0k}\bar{x}(n) + w^H(n)M_{0k}w(n)\right)$$
$$\approx -\frac{1}{N}\sum_{n=1}^{N}\left(\bar{x}^H(n)M_{0k}w(n) + w^H(n)M_{0k}\bar{x}(n)\right.$$
$$\left. + w^H(n)M_{0k}w(n)\right)$$
$$\triangleq \mu_{k1} + \mu_{k2} + \mu_{k3} \quad (\text{A12})$$

where

$$\mu_{k1} = -\frac{1}{N}\sum_{n=1}^{N}\bar{x}^H(n)M_{0k}w(n) \quad (\text{A13})$$

$$\mu_{k2} = -\frac{1}{N}\sum_{n=1}^{N}w(n)^H M_{0k}\bar{x}(n) \quad (\text{A14})$$

$$\mu_{k3} = -\frac{1}{N}\sum_{n=1}^{N}w^H(n)M_{0k}w(n). \quad (\text{A15})$$

Then from (A12), the two terms of $\text{MSE}(\hat{\theta}_k)$ in (A11) can be obtained as

$$E\{\mu_k^2\} = E\{\mu_{k1}^2 + \mu_{k2}^2 + \mu_{k3}^2 + 2\mu_{k1}\mu_{k2}$$
$$+ 2\mu_{k1}\mu_{k3} + 2\mu_{k2}\mu_{k3}\} \quad (\text{A16})$$

$$E\{|\mu_k|^2\} = E\{|\mu_{k1}|^2 + |\mu_{k2}|^2 + |\mu_{k3}|^2$$
$$+ \text{Re}\{2\mu_{k1}\mu_{k2}^* + 2\mu_{k1}\mu_{k3}^* + 2\mu_{k2}\mu_{k3}^*\}\}. \quad (\text{A17})$$

Under the basic assumptions on the data model and the well-known formula for the expectation of four Gaussian random variables with zero-mean (e.g., [60])

$$E\{Abc^T D\} = E\{Ab\}E\{c^T D\} + E\{c^T \otimes A\}$$
$$\cdot E\{D \otimes b\} + E\{AE\{bc^T\}D\} \quad (\text{A18})$$

from (A12), we can get

$$E\{\mu_{k1}^2\}$$
$$= \frac{1}{N^2}E\left\{\sum_{n=1}^{N}\sum_{t=1}^{N}\bar{x}^H(n)M_{0k}w(n)\bar{x}^H(t)M_{0k}w(t)\right\}$$
$$= 0 \quad (\text{A19})$$

$$E\{\mu_{k2}^2\}$$
$$= \frac{1}{N^2}E\left\{\sum_{n=1}^{N}\sum_{t=1}^{N}w^H(n)M_{0k}\bar{x}(n)w^H(t)M_{0k}\bar{x}(t)\right\}$$
$$= 0 \quad (\text{A20})$$

$$B_m = \begin{bmatrix} e_{\bar{K}+m_2}^T e_{2M+2-\bar{K}-m_1}, & e_{\bar{K}-1+m_2}^T e_{2M+3-\bar{K}-m_1}, & \cdots & e_{1+i_2}^T e_{2M+1-m_1} \\ e_{\bar{K}+1+m_2}^T e_{2M+1-\bar{K}-m_1}, & e_{\bar{K}+m_2}^T e_{2M+2-\bar{K}-m_1}, & \cdots & e_{2+m_2}^T e_{2M-m_1} \\ \vdots & \vdots & \ddots & \vdots \\ e_{2M+1+m_2}^T e_{1-m_1}, & e_{2M+m_2}^T e_{2-m_1} & \cdots & e_{2M+2+m_2}^T e_{\bar{K}-m_1} \end{bmatrix} \quad (\text{A9})$$

$E\{\mu_{k3}^2\}$

$$= \frac{1}{N^2} E \left\{ \sum_{n=1}^{N} \sum_{t=1}^{N} \boldsymbol{w}^H(n) \boldsymbol{M}_{0k} \boldsymbol{w}(n) \boldsymbol{w}^H(t) \boldsymbol{M}_{0k} \boldsymbol{w}(t) \right\}$$

$$= \frac{\sigma^4}{N} \text{tr}\{\boldsymbol{M}_{0k} \boldsymbol{M}_{0k}\} \tag{A21}$$

$E\{\mu_{k1}\mu_{k2}\}$

$$= \frac{1}{N^2} E \left\{ \sum_{n=1}^{N} \sum_{t=1}^{N} \bar{\boldsymbol{x}}^H(n) \boldsymbol{M}_{0k} \boldsymbol{w}(n) \boldsymbol{w}^H(t) \boldsymbol{M}_{0k} \bar{\boldsymbol{x}}(t) \right\}$$

$$= \frac{\sigma^2}{N} \text{tr}\{\boldsymbol{M}_{0k} \bar{\boldsymbol{R}} \boldsymbol{M}_{0k}\} \tag{A22}$$

$E\{\mu_{k1}\mu_{k3}\}$

$$= \frac{1}{N^2} E \left\{ \sum_{n=1}^{N} \sum_{t=1}^{N} \bar{\boldsymbol{x}}^H(n) \boldsymbol{M}_{0k} \boldsymbol{w}(n) \boldsymbol{w}^H(n) \boldsymbol{M}_{0k} \boldsymbol{w}(n) \right\}$$

$$= 0 \tag{A23}$$

$E\{\mu_{k2}\mu_{k3}\}$

$$= \frac{1}{N^2} E \left\{ \sum_{n=1}^{N} \sum_{t=1}^{N} \boldsymbol{w}^H(n) \boldsymbol{M}_{0k} \bar{\boldsymbol{x}}(n) \boldsymbol{w}^H(t) \boldsymbol{M}_{0k} \boldsymbol{w}(t) \right\}$$

$$= 0. \tag{A24}$$

Similarly, we have

$$E\{|\mu_{k1}|^2\} = \frac{\sigma^2}{N} \text{tr}\{\boldsymbol{M}_{0k}^H \bar{\boldsymbol{R}} \boldsymbol{M}_{0k}\} \tag{A25}$$

$$E\{|\mu_{k2}|^2\} = \frac{\sigma^2}{N} \text{tr}\{\boldsymbol{M}_{0k} \bar{\boldsymbol{R}} \boldsymbol{M}_{0k}^H\} \tag{A26}$$

$$E\{|\mu_{k3}|^2\} = \frac{\sigma^4}{N} \text{tr}\{\boldsymbol{M}_{0k} \boldsymbol{M}_{0k}^H\} \tag{A27}$$

$$E\{\mu_{k1}\mu_{k2}^*\} = E\{\mu_{k1}\mu_{k3}^*\} = E\{\mu_{k2}\mu_{k3}^*\} = 0 \tag{A28}$$

where the facts $\text{tr}\{\boldsymbol{M}_{0k}\} = 0$, $(\boldsymbol{A} \otimes \boldsymbol{B})(\boldsymbol{C} \otimes \boldsymbol{D}) = (\boldsymbol{AC}) \otimes (\boldsymbol{BD})$ and $(\boldsymbol{A} \otimes \boldsymbol{B})^T = \boldsymbol{A}^T \otimes \boldsymbol{B}^T$ are used. Therefore by substituting (A19)–(A28) into (A11) and performing some straightforward manipulations, the asymptotic MSE expression $\text{MSE}(\hat{\theta}_k)$ in (46) of the estimated DOAs of the NF signals can be readily obtained. ∎

APPENDIX B
PROOF OF THEOREM 2

Similar to the derivations for the DOAs in Appendix A, the estimation $\hat{r}_k$ is minimum point of $f_{\bar{m}}(\hat{\theta}_k, r)$ in (24), we get [66]

$$f'_{\bar{m}r}(\hat{\theta}_k, \hat{r}_k) = 0 \tag{B1}$$

where $f'_{\bar{m}r}(\theta, r)$ is the first-order partial derivative of $f_{\bar{m}}(\theta, r)$ with respect to r given by

$$f'_{\bar{m}r}(\hat{\theta}_k, \hat{r}_k) \triangleq \frac{\partial f_{\bar{m}}(\theta, r)}{\partial r}$$

$$= 2\text{Re}\{\boldsymbol{d}_{\bar{m}}^H \theta, r) \boldsymbol{\Pi}_{\hat{Q}_{\bar{m}}} \boldsymbol{a}_{\bar{m}}(\theta, r)\}. \tag{B2}$$

Since $\hat{\theta}_k$ and $\hat{r}_k$ are consistent estimates for a sufficiently large number of snapshots N, the approximation of $f'_{\bar{m}r}(\hat{\theta}_k, \hat{r}_k)$ can be found in its Taylors series expansion about the true value θ_k and r_k as

$$f'_{\bar{m}r}(\hat{\theta}_k, \hat{r}_k) \approx f'_{\bar{m}r}(\theta_k, r_k) + f''_{\bar{m}rr}(\theta_k, r_k)(\hat{r}_k - r_k)$$

$$+ f''_{\bar{m}r\theta}(\theta_k, r_k)(\hat{\theta}_k - \theta_k) \tag{B3}$$

where the second-order partial derivatives $f''_{\bar{m}rr}(\theta_k, r_k)$ and $f''_{\bar{m}r\theta}(\theta_k, r_k)$ of $f_{\bar{m}}(\theta_k, r_k)$ are given by [59], [66]

$$f''_{\bar{m}rr}(\theta, r) \triangleq \frac{\partial f'_{\bar{m}r}(\theta, r)}{\partial r}$$

$$= 2\text{Re}\{\bar{\boldsymbol{d}}_{\bar{m}rr}^H(\theta, r) \boldsymbol{\Pi}_{\hat{Q}_{\bar{m}}} \boldsymbol{a}_{\bar{m}}(\theta, r)$$

$$+ \boldsymbol{d}_{\bar{m}r}^H(\theta, r) \boldsymbol{\Pi}_{\hat{Q}_{\bar{m}}} \boldsymbol{d}_{\bar{m}r}(\theta, r)\}$$

$$\approx 2\text{Re}\{\boldsymbol{d}_{\bar{m}r}^H(\theta, r) \boldsymbol{\Pi}_{\hat{Q}_{\bar{m}}} \boldsymbol{d}_{\bar{m}r}(\theta, r)\} \tag{B4}$$

$$f''_{\bar{m}r\theta}(\theta, r) \triangleq \frac{\partial f'_{\bar{m}r}(\theta, r)}{\partial \theta}$$

$$= 2\text{Re}\{\bar{\boldsymbol{d}}_{\bar{m}r\theta}^H(\theta, r) \boldsymbol{\Pi}_{\hat{Q}_{\bar{m}}} \boldsymbol{a}_{\bar{m}}(\theta, r)$$

$$+ \boldsymbol{d}_{\bar{m}r}^H(\theta, r) \boldsymbol{\Pi}_{\hat{Q}_{\bar{m}}} \boldsymbol{d}_{\bar{m}\theta}(\theta, r)\}$$

$$\approx 2\text{Re}\{\boldsymbol{d}_{\bar{m}r}^H(\theta, r) \boldsymbol{\Pi}_{\hat{Q}_{\bar{m}}} \boldsymbol{d}_{\bar{m}\theta}(\theta, r)\}. \tag{B5}$$

Thus we can obtain the estimate error $\Delta r_k \triangleq \hat{r}_k - r_k$ as

$$\Delta r_k \triangleq \hat{r}_k - r_k$$

$$\approx - \frac{1}{f''_{\bar{m}rr}(\theta_k, r_k)}$$

$$\cdot \left(f'_{\bar{m}r}(\theta_k, r_k) - f''_{\bar{m}r\theta}(\theta_k, r_k) \frac{\text{Re}\{\mu_k\}}{H_{0kk}} \right)$$

$$\approx - \frac{1}{\boldsymbol{d}_{\bar{m}r}^H(\theta, r) \boldsymbol{\Pi}_{Q_{\bar{m}}} \boldsymbol{d}_{\bar{m}r}(\theta, r)}$$

$$\cdot \left(\text{Re}\{\boldsymbol{d}_{\bar{m}}^H(\theta, r) \boldsymbol{\Pi}_{\hat{Q}_{\bar{m}}} \boldsymbol{a}_{\bar{m}}(\theta, r)\} \right.$$

$$\left. - \text{Re}\{\boldsymbol{d}_{\bar{m}r}^H(\theta, r) \boldsymbol{\Pi}_{Q_{\bar{m}}} \boldsymbol{d}_{\bar{m}\theta}(\theta, r)\} \frac{\text{Re}\{\mu_k\}}{H_{0kk}} \right)$$

$$= - \frac{1}{H_{\bar{m}kk}} \left(\text{Re}\{\xi_k\} + \bar{H}_{\bar{m}kk} \frac{\text{Re}\{\mu_k\}}{H_{0kk}} \right) \tag{B6}$$

where the estimated orthogonal projector $\boldsymbol{\Pi}_{\hat{Q}_{\bar{m}}}$ in the second-order derivatives $f''_{\bar{m}rr}(\theta_k, r_k)$ and $f''_{\bar{m}r\theta}(\theta_k, r_k)$ are replaced with the true $\boldsymbol{\Pi}_{Q_{\bar{m}}}$ without affecting the asymptotic property of estimates $\hat{r}_k$ similarly to that used in [66], and

$$\xi_k \triangleq \boldsymbol{d}_{\bar{m}}^H(\theta_k, r_k) \boldsymbol{\Pi}_{\hat{Q}_{\bar{m}}} \boldsymbol{a}_{\bar{m}}(\theta_k, r_k). \tag{B7}$$

Similarly to the derivations for the DOAs in (A1)–(A6), we have

$$\xi_k = - \boldsymbol{d}_{\bar{m}}^H(\theta_k, r_k) \boldsymbol{\Pi}_{Q_{\bar{m}}} \hat{\boldsymbol{Z}}_{\bar{m}} \boldsymbol{Z}_{\bar{m}1}^H (\boldsymbol{Z}_{\bar{m}1} \boldsymbol{Z}_{\bar{m}1}^H)^{-1} \boldsymbol{a}_{\bar{m}1}(\theta_k, r_k)$$

$$= - \boldsymbol{g}_{\bar{m}}^H(\theta_k, r_k) \hat{\boldsymbol{Z}}_{\bar{m}} \boldsymbol{h}_{\bar{m}}(\theta_k, r_k). \tag{B8}$$

By substituting (A8) into (B8), we get

$$\xi_k = -\frac{1}{N}\sum_{n=1}^{N} \boldsymbol{g}_{\bar{m}}^H(\theta_k, r_k)(\boldsymbol{I}_L \otimes \boldsymbol{x}^H(n))$$
$$\cdot \boldsymbol{C}_{\bar{m}}(\boldsymbol{I}_{\bar{K}} \otimes \boldsymbol{x}(n))\boldsymbol{h}_{\bar{m}}(\theta_k, r_k)$$
$$= -\frac{1}{N}\sum_{n=1}^{N} \boldsymbol{x}^H(n)(\boldsymbol{g}_{\bar{m}}^H(\theta_k, r_k) \otimes \boldsymbol{I}_{2M+1})$$
$$\cdot \boldsymbol{C}_{\bar{m}}(\boldsymbol{h}_{\bar{m}}(\theta_k, r_k) \otimes \boldsymbol{I}_{2M+1})\boldsymbol{x}(n)$$
$$= -\frac{1}{N}\sum_{n=1}^{N} \boldsymbol{x}^H(n)\boldsymbol{M}_{\bar{m}k}\boldsymbol{x}(n) \tag{B9}$$

Thus from (B6) and (A11), the MSE (or variance) of the estimation error $\Delta\hat{r}_k$ is given by

$$\mathrm{MSE}(\hat{r}_k) \triangleq E\{(\Delta r_k)^2\} = \mathrm{var}(\hat{r}_k)$$
$$\approx \frac{\bar{H}_{\bar{m}kk}^2}{H_{\bar{m}kk}^2}\mathrm{MSE}(\hat{\theta}_k)$$
$$+ \frac{1}{2H_{\bar{m}kk}^2}\mathrm{Re}\{E\{\xi_k^2\} + E\{|\xi_k|^2\}\}$$
$$+ \frac{\bar{H}_{\bar{m}kk}}{H_{\bar{m}kk}^2 H_{0kk}}\mathrm{Re}\{E\{\xi_k\mu_k\} + E\{\xi_k\mu_k^*\}\}. \tag{B10}$$

Similarly by substituting the relation $\boldsymbol{x}(n) = \bar{\boldsymbol{x}}(n) + \boldsymbol{w}(n)$ (i.e., $\bar{\boldsymbol{x}}(n) \triangleq \boldsymbol{A}\boldsymbol{s}(n)$) into (B9), we can rewrite ξ_k in (B9) as

$$\xi_k = -\frac{1}{N}\sum_{n=1}^{N}\big(\bar{\boldsymbol{x}}^H(n)\boldsymbol{M}_{\bar{m}k}\bar{\boldsymbol{x}}(n) + \bar{\boldsymbol{x}}^H(n)\boldsymbol{M}_{\bar{m}k}\boldsymbol{w}(n)$$
$$+ \boldsymbol{w}^H(n)\boldsymbol{M}_{\bar{m}k}\bar{\boldsymbol{x}}(n) + \boldsymbol{w}^H(n)\boldsymbol{M}_{\bar{m}k}\boldsymbol{w}(n)\big)$$
$$\approx -\frac{1}{N}\sum_{n=1}^{N}\big(\bar{\boldsymbol{x}}^H(n)\boldsymbol{M}_{\bar{m}k}\boldsymbol{w}(n) + \boldsymbol{w}^H(n)\boldsymbol{M}_{\bar{m}k}\bar{\boldsymbol{x}}(n)$$
$$+ \boldsymbol{w}^H(n)\boldsymbol{M}_{\bar{m}k}\boldsymbol{w}(n)\big)$$
$$\triangleq \xi_{k1} + \xi_{k2} + \xi_{k3} \tag{B11}$$

where

$$\xi_{k1} = -\frac{1}{N}\sum_{n=1}^{N}\bar{\boldsymbol{x}}^H(n)\boldsymbol{M}_{\bar{m}k}\boldsymbol{w}(n) \tag{B12}$$

$$\xi_{k2} = -\frac{1}{N}\sum_{n=1}^{N}\boldsymbol{w}(n)^H\boldsymbol{M}_{\bar{m}k}\bar{\boldsymbol{x}}(n) \tag{B13}$$

$$\xi_{k3} = -\frac{1}{N}\sum_{n=1}^{N}\boldsymbol{w}^H(n)\boldsymbol{M}_{\bar{m}k}\boldsymbol{w}(n). \tag{B14}$$

Then from (B11), the last four terms of $\mathrm{MSE}(\hat{r}_k)$ in (B10) can be obtained as

$$E\{\xi_k^2\} = E\{\xi_{k1}^2 + \xi_{k2}^2 + \xi_{k3}^2 + 2\xi_{k1}\xi_{k2}$$
$$+ 2\xi_{k1}\xi_{k3} + 2\xi_{k2}\xi_{k3}\} \tag{B15}$$
$$E\{|\xi_k|^2\} = E\{|\xi_{k1}|^2 + |\xi_{k2}|^2 + |\xi_{k3}|^2$$
$$+ \mathrm{Re}\{2\xi_{k1}\xi_{k2}^* + 2\xi_{k1}\xi_{k3}^* + 2\xi_{k2}\xi_{k3}^*\}\} \tag{B16}$$

$$E\{\xi_k\mu_k\} = E\{\xi_{k1}\mu_{k1} + \xi_{k1}\mu_{k2} + \xi_{k1}\mu_{k3}$$
$$+ \xi_{k2}\mu_{k1} + \xi_{k2}\mu_{k2} + \xi_{k2}\mu_{k3}$$
$$+ \xi_{k3}\mu_{k1} + \xi_{k3}\mu_{k2} + \xi_{k3}\mu_{k3}\} \tag{B17}$$
$$E\{\xi_k\mu_k^*\} = E\{\xi_{k1}\mu_{k1}^* + \xi_{k1}\mu_{k2}^* + \xi_{k1}\mu_{k3}^*$$
$$+ \xi_{k2}\mu_{k1}^* + \xi_{k2}\mu_{k2}^* + \xi_{k2}\mu_{k3}^*$$
$$+ \xi_{k3}\mu_{k1}^* + \xi_{k3}\mu_{k2}^* + \xi_{k3}\mu_{k3}^*\}. \tag{B18}$$

Hence similarly to the analysis in Appendix A, we have

$$E\{\xi_{k1}^2\} = E\{\xi_{k2}^2\} = 0 \tag{B19}$$

$$E\{\xi_{k3}^2\} = \frac{\sigma^4}{N}\mathrm{tr}\{\boldsymbol{M}_{\bar{m}k}\boldsymbol{M}_{\bar{m}k}\} \tag{B20}$$

$$E\{\xi_{k1}\xi_{k2}\} = \frac{\sigma^2}{N}\mathrm{tr}\{\boldsymbol{M}_{\bar{m}k}\bar{\boldsymbol{R}}\boldsymbol{M}_{\bar{m}k}\} \tag{B21}$$

$$E\{\xi_{k1}\xi_{k3}\} = E\{\xi_{k2}\xi_{k3}\} = 0 \tag{B22}$$

$$E\{|\xi_{k1}|^2\} = \frac{\sigma^2}{N}\mathrm{tr}\{\boldsymbol{M}_{\bar{m}k}^H\bar{\boldsymbol{R}}\boldsymbol{M}_{\bar{m}k}\} \tag{B23}$$

$$E\{|\xi_{k2}|^2\} = \frac{\sigma^2}{N}\mathrm{tr}\{\boldsymbol{M}_{\bar{m}k}\bar{\boldsymbol{R}}\boldsymbol{M}_{\bar{m}k}^H\} \tag{B24}$$

$$E\{|\xi_{k3}|^2\} = \frac{\sigma^4}{N}\mathrm{tr}\{\boldsymbol{M}_{\bar{m}k}\boldsymbol{M}_{\bar{m}k}^H\} \tag{B25}$$

$$E\{\xi_{k1}\xi_{k2}^*\} = E\{\xi_{k1}\xi_{k3}^*\} = E\{\xi_{k2}\xi_{k3}^*\} = 0. \tag{B26}$$

Additionally, we easily get

$$E\{\xi_{k1}\mu_{k1}\} = E\{\xi_{k2}\mu_{k2}\} = E\{\xi_{k3}\mu_{k2}\} = 0 \tag{B27}$$

$$E\{\xi_{k3}\mu_{k3}\} = \frac{\sigma^4}{N}\mathrm{tr}\{\boldsymbol{M}_{\bar{m}k}\boldsymbol{M}_{0k}\} \tag{B28}$$

$$E\{\xi_{k1}\mu_{k2}\} = \frac{\sigma^2}{N}\mathrm{tr}\{\boldsymbol{M}_{\bar{m}k}\bar{\boldsymbol{R}}\boldsymbol{M}_{0k}\} \tag{B29}$$

$$E\{\xi_{k2}\mu_{k1}\} = \frac{\sigma^2}{N}\mathrm{tr}\{\boldsymbol{M}_{\bar{m}k}\bar{\boldsymbol{R}}\boldsymbol{M}_{0k}\} \tag{B30}$$

$$E\{\xi_{k1}\mu_{k3}\} = E\{\xi_{k2}\mu_{k3}\} = E\{\xi_{k3}\mu_{k1}\} = 0 \tag{B31}$$

$$E\{\xi_{k1}\mu_{k1}^*\} = \frac{\sigma^2}{N}\mathrm{tr}\{\boldsymbol{M}_{\bar{m}k}^H\bar{\boldsymbol{R}}\boldsymbol{M}_{0k}\} \tag{B32}$$

$$E\{\xi_{k2}\mu_{k2}^*\} = \frac{\sigma^2}{N}\mathrm{tr}\{\boldsymbol{M}_{\bar{m}k}\bar{\boldsymbol{R}}\boldsymbol{M}_{0k}^H\} \tag{B33}$$

$$E\{\xi_{k3}\mu_{k3}^*\} = \frac{\sigma^4}{N}\mathrm{tr}\{\boldsymbol{M}_{\bar{m}k}\boldsymbol{M}_{0k}^H\} \tag{B34}$$

$$E\{\xi_{k1}\mu_{k2}^*\} = E\{\xi_{k1}\mu_{k3}^*\} = E\{\xi_{k2}\mu_{k3}^*\} = 0 \tag{B35}$$
$$E\{\xi_{k2}\mu_{k1}^*\} = E\{\xi_{k3}\mu_{k2}^*\} = E\{\xi_{k3}\mu_{k1}^*\} = 0. \tag{B36}$$

Therefore by inserting (B19)–(B36) into (B10), and performing some straightforward manipulations, $\mathrm{MSE}(\hat{r}_k)$ of the estimated ranges of the NF signals can be readily obtained. ∎

References

[1] S. Pasupathy and W. J. Alford, "Range and bearing estimation in passive sonar," *IEEE Trans. Aerosp. Electron. Syst.*, vol. AES-16, no. 2, pp. 244–249, Mar. 1980.

[2] D. H. Johnson and D. E. Dudgeon, *Array Signal Processing: Concepts and Techniques.* Upper Saddle River, NJ, USA: Prentice Hall, 1993.

[3] H. Krim and M. Viberg, "Two decades of array signal processing research: The parametric approach," *IEEE Signal Process. Mag.*, vol. 13, no. 4, pp. 67–94, Jul. 1996.

[4] P. R. P. Hoole, Ed., *Smart Antennas and Signal Processing for Communications, Biomedical and Radar Systems.* Southampton, U.K.: WIT Press, 2001.

[5] J. C. Chen, K. Yao, and R. Hudson, "Source localization and beamforming," *IEEE Signal Process. Mag.*, vol. 19, no. 2, pp. 30–39, Mar. 2002.

[6] J. Capon, "High resolution frequency-Wavenumber spectrum analysis," *Proc. IEEE,* vol. 57, no. 8, pp. 1408–1418, Aug. 1969.

[7] D. Salvati, C. Drioli, and G. L. Foresti, "A low-complexity robust beamforming using diagonal unloading for acoustic source localization," *IEEE/ACM Trans. Audio, Speech, Lang. Process.*, vol. 26, no. 3, pp. 609–622, Mar. 2018.

[8] D. Salvati, C. Drioli, and G. L. Foresti, "Exploiting CNNs for improving acoustic source localization in noisy and reverberant conditions," *IEEE Trans. Emerg. Topics Comput. Intell.*, vol. 2, no. 2, pp. 103–116, Apr. 2018.

[9] H. Wang and M. Kaveh, "Coherent signal-subspace processing for the detection and estimation of angles of arrival of multiple wide-band sources," *IEEE Trans. Acoust., Speech, Signal Process.*, vol. ASSP-33, no. 4, pp. 823–831, Aug. 1985.

[10] E. D. Claudio and R. Parisi, "WAVES: Weighted average of signal subspaces for robust wideband direction finding," *IEEE Trans. Signal Process.*, vol. 49, no. 10, pp. 2179–2191, Oct. 2001.

[11] J. C. Chen, K. Yao, and R. E. Hudson, "Acoustic source localization and beamforming: Theory and practice," *EURASIP J. Adv. Signal Process.*, vol. 4, pp. 359–370, 2003.

[12] T. Li and A. Nehorai, "Direction-of-arrival estimation of hydroacoustic signals from marine vessels containing random and sinusoidal components," *IEEE Signal Process. Lett.*, vol. 19, no. 8, pp. 503–506, Aug. 2012.

[13] Y. I. Wu and K. T. Wong, "Acoustic near-field source-localization by two passive anchor-nodes," *IEEE Trans. Aerosp. Electron. Syst.*, vol. 48, no. 1, pp. 159–169, Jan. 2012.

[14] L. Lu, H. C. Wu, K. Yan, and S. S. Iyengar, "Robust expectation-maximization algorithm for multiple wideband acoustic source localization in the presence of nonuniform noise variances," *IEEE Sens. J.*, vol. 11, no. 3, pp. 536–544, Mar. 2011.

[15] E. Dranka and R. Coelho, "Robust maximum likelihood acoustic energy based source localization in correlated noisy sensing environments," *IEEE J. Sel. Topics Signal Process.*, vol. 9, no. 2, pp. 259–267, Mar. 2015.

[16] V. F. Pisarenko, "The retrieval of harmonics from a covariance function," *Geophys. J. Roy. Astron. Soc.*, vol. 33, pp. 347–366, 1973.

[17] R. O. Schmidt, "Multiple emitter location and signal parameter estimation," in *Proc. RADC Spectr. Estimation Workshop*, Rome, NY, USA, Oct. 1979, pp. 243–258.

[18] R. Kumaresan and D. W. Tufts, "Estimating the angels of arrival of multiple plane waves," *IEEE Trans. Aerosp. Electron. Syst.*, vol. 19, no. 1, pp. 134–139, Jan. 1983.

[19] R. Roy and T. Kalaith, "ESPRIT—Estimation of signal parameters via rational invariance techniques," *IEEE Trans. Acoust., Speech, Signal Process.*, vol. 37, no. 7, pp. 984–995, Jul. 1989.

[20] P. Stoica and A. Nehorai, "MUSIC, maximum likelihood, and Cramer–Rao bound," *IEEE Trans. Acoust., Speech, Signal Process.*, vol. 37, no. 5, pp. 720–741, May 1989.

[21] P. Stoica and K. C. Sharman, "Maximum likelihood methods for direction-of-arrival estimation," *IEEE Trans. Acoust., Speech, Signal Process.*, vol. 38, no. 7, pp. 1132–1143, Jul. 1990.

[22] M. Viberg and B. Ottersten, "Sensor array processing based on subspace fitting," *IEEE Trans. Signal Process.*, vol. 39, no. 5, pp. 1110–1121, May 1991.

[23] Y.-D. Huang and M. Barkat, "Near-field multiple source localization by passive sensor array," *IEEE Trans. Antennas Propag.*, vol. 39, no. 7, pp. 968–975, Jul. 1991.

[24] A. J. Weiss and B. Friedlander, "Range and bearing estimation using polynomial rooting," *IEEE J. Ocean. Eng.*, vol. 18, no. 2, pp. 130–137, Apr. 1993.

[25] J. C. Chen, R. E. Hudson, and K. Yao, "Maximum-likelihood source localization and unknown sensor location estimation for wideband signals in the near-field," *IEEE Trans. Signal Process.*, vol. 50, no. 8, pp. 1843–1854, Aug. 2002.

[26] E. Boyer, A. Ferreol, and P. Larzabal, "Simple robust bearing-range source's localization with curved wavefronts," *IEEE Signal Process. Lett.*, vol. 12, no. 6, pp. 457–460, Jun. 2005.

[27] L. Kumar and R. M. Hegde, "Near-field acoustic source localization and beamforming in spherical harmonics domain," *IEEE Trans. Signal Process.*, vol. 64, no. 13, pp. 3351–3361, Jul. 2016.

[28] A. L. Swindlehurst and T. Kailath, "Passive direction-of-arrival and range estimation for near-field sources," in *Proc. IEEE 4th ASSP Workshop Spectr. Estimation Model.*, Minneapolis, MN, USA, Aug. 1988, pp. 123–128.

[29] D. Starer and A. Nehorai, "Passive localization of near-field sources by path following," *IEEE Trans. Signal Process.*, vol. 42, no. 3, pp. 677–680, Mar. 1994.

[30] J. Lee, C. Lee, and K. Lee, "A modified path-following algorithm using a known algebraic path," *IEEE Trans. Signal Process.*, vol. 47, no. 5, pp. 1407–1409, May 1999.

[31] R. N. Challa and S. Shamsunder, "High-order subspace-based algorithms for passive localization of near-field sources," in *Proc. IEEE 29th Asilomar Conf. Signals, Syst., Comput.*, vol. 2, Pacific Grove, CA, USA, Nov. 1995, pp. 777–781.

[32] N. Yuen and B. Friedlander, "Performance analysis of higher order ESPRIT for localization of near-field sources," *IEEE Trans. Signal Process.*, vol. 46, no. 3, pp. 709–719, Mar. 1998.

[33] Y. Wu, L. Ma, C. Hou, G. Zhang, and J. Li, "Subspace-based method for joint range and DOA estimation of multiple near-field sources," *Signal Process.*, vol. 86, no. 8, pp. 2129–2133, 2006.

[34] J. Liang, X. Zeng, B. Ji, J. Zhang, and F. Zhao "A computationally efficient algorithm for joint range-DOA-frequency estimation of near-field sources," *Digit. Signal Process.*, vol. 19, no. 4, pp. 596–611, 2009.

[35] H. Chen, X. Zhang, Y. Bai, and J. Ma, "Computationally efficient DOA and range estimation for near-field source with linear antenna array," in *Proc. World Congr. Eng. Comput. Sci.*, vol. 1, San Francisco, CA, USA, Oct. 2017, pp. 412–415.

[36] Y. S. Hsu, K. T. Wong, and L. Yeh, "Mismatch of near-field bearing-range spatial geometry in source-localization by a uniform linear array," *IEEE Trans. Antennas Propag.*, vol. 59, no. 10, pp. 3658–3667, Oct. 2011.

[37] P. Singh, Y. Wang, and P. Chargè, "A correction method for the near field approximated model based localization techniques," *Digit. Signal Process.*, vol. 67, pp. 76–80, 2017.

[38] H. Gazzah and J. P. Delmas, "CRB-based design of linear antenna arrays for near-field source localization," *IEEE Trans. Antennas Propag.*, vol. 62, no. 4, pp. 1965–1974, Apr. 2014.

[39] M. Haardt, R. N. Challa, and S. Shamsunder, "Improved bearing and range estimation via high-order subspace based unitary esprit," in *Proc. IEEE 30th Asilomar Conf. Signals, Syst. Comput.*, vol. 1, Pacific Grove, CA, USA, 1996, pp. 380–384.

[40] J. H. Lee and C. H. Tung, "Estimating the bearings of near-field cyclostationary signals," *IEEE Trans. Signal Process.*, vol. 50, no. 1, pp. 110–118, Jan. 2002.

[41] J. Liang and D. Liu, "Passive localization of near-field sources using cumulant," *IEEE Sens. J.*, vol. 9, no. 8, pp. 953–960, Aug. 2009.

[42] J. Li *et al.*, "Simplified high-order DOA and range estimation with linear antenna array," *IEEE Commun. Lett.*, vol. 21, no. 1, pp. 76–79, Jan. 2017.

[43] J. Lee, Y. Chen, and C. Yeh, "A covariance approximation method for near-field direction-finding using a uniform linear array," *IEEE Trans. Signal Process.*, vol. 43, no. 5, pp. 1293–1298, May 1995.

[44] E. Grosicki, K. Meraim, and Y. Hua, "A weighted linear prediction method for near-field source localization," *IEEE Trans. Signal Process.*, vol. 53, no. 10, pp. 3651–3660, Oct. 2005.

[45] W. Zhi and M. Y. W. Chia, "Near-field source localization via symmetric subarrays," *IEEE Signal Process. Lett.*, vol. 14, no. 6, pp. 409–412, Jun. 2007.

[46] R. Boyer and J. Picheral, "Second-order near-field localization with automatic paring operation," in *Proc. IEEE Int. Conf. Acoust., Speech, Signal Process.*, Las Vegas, NV, USA Mach 2008, pp. 2569–2572.

[47] J. W. Tao, L. Liu, and Z.-Y. Lin, "Joint DOA, range, and polarization estimation in the Fresnel region," *IEEE Trans. Aerosp. Electron. Syst.*, vol. 47, no. 4, pp. 2657–2672, Oct. 2011.

[48] X. Zhang, W. Chen, W. Zheng, Z. Xia, and Y. Wang, "Localization of near-field sources: A reduced-dimension MUSIC algorithm," *IEEE Commun. Lett.*, vol. 22, no. 7, pp. 1422–1425, Jul. 2018.

[49] K. Hu, S. P. Chepuri, and G. Leus, "Near-field source localization: Sparse recovery techniques and grid matching," in *Proc. IEEE 8th Sens. Array Multichannel Signal Process. Workshop*, A Coruna, Spain, Jun. 2014, pp. 369–372.

[50] J. Benesty, "Adaptive eigenvalue decomposition algorithm for passive acoustic source localization," *J. Acoust. Soc. Amer.*, vol. 107, no. 1, pp. 384–390, 2000.

[51] P. Comon and G. H. Golub, "Tracking a few extreme singular values and vectors in signal processing," *Proc. IEEE*, vol. 78, no. 8, p. 1327–1343, Aug. 1990.

[52] J. Xin and A. Sano, "Efficient subspace-based algorithm for adaptive bearing estimation and tracking," *IEEE Trans. Signal Process.*, vol. 53, no. 12, pp. 4485–4505, Dec. 2005.

[53] F. Gao and A. B. Gershman, "A generalized ESPRIT approach to direction-of-arrival estimation," *IEEE Signal Process. Lett.*, vol. 12, no. 3, pp. 254–257, Mar. 2005.

[54] G. Wang, J. Xin, J. Wu, J. Wang, N. Zheng, and A. Sano, "New generalized ESPRIT for direction estimation and its mathematical link to RARE method," in *Proc. IEEE 12th Int. Conf. Signal Process.*, Beijing, China, Oct. 2012, pp. 360–363.

[55] W. Zuo, J. Xin, G. Wang, J. Wang, N. Zheng, and A. Sano, "Near-field source localization with partly sensor gain and phase uncertainties," in *Proc. IEEE 15th Int. Workshop Signal Process. Adv. Wireless Commun.*, Toronto, Canada, Jun. 2014, pp. 160–164.

[56] S. Marcos, A. Marsal, and M. Benider, "The propagator method for sources bearing estimation," *Signal Process.*, vol. 42, pp. 121–138, 1995.

[57] J. Sanchez-Araujo and S. Marcos, "Statistical analysis of the propagator method for DOA estimation without eigendecomposition," in *Proc. IEEE 8th Workshop Statist. Signal Array Process.*, Corfu, Greece, Jun. 1996, pp. 570–573.

[58] J. Xin and A. Sano, "Direction estimation of coherent signals using spatial signature," *IEEE Signal Process. Lett.*, vol. 9, no. 12, pp. 414–417, Dec. 2002.

[59] J. Xin and A. Sano, "Computationally efficient subspace-based method for direction-of-arrival estimation without eigendecomposition," *IEEE Trans. Signal Process.*, vol. 52, no. 4, pp. 876–893, Apr. 2004.

[60] P. H. M. Janssen and P. Stoica, "On the expectation of the product of four matrix-valued Gaussian random variables," *IEEE Trans. Autom. Control*, vol. 33, no. 9, pp. 867–870, Sep. 1988.

[61] P. Stoica and T. Söderström, "Statistical analysis of a subspace method for bearing estimation without eigendecomposition," *IEE Proc. F-Radar Signal Process.*, vol. 139, no. 4, pp. 301–305, Aug. 1992.

[62] G. Wang, J. Xin, N. Zheng, and A. Sano, "Computationally efficient subspace-based method for two-dimensional direction estimation with L-shaped array," *IEEE Trans. Signal Process.*, vol. 59, no. 7, pp. 3197–3212, Jul. 2011.

[63] R. Boyer and G. Bouleux, "Oblique projections for direction-of-arrival estimation with prior knowledge," *IEEE Trans. Signal Process.*, vol. 56, no. 4, pp. 1374–1387, Apr. 2008.

[64] C. R. Rao, C. R. Sastry, and B. Zhou, "Tracking the direction of arrival of multiple moving targets," *IEEE Trans. Signal Process.*, vol. 42, no. 5, pp. 1133–1144, May 1994.

[65] J. Xin, N. Zheng, and A. Sano, "Subspace-based adaptive method for estimating direction-of-arrival with Luenberger observer," *IEEE Trans. Signal Process.*, vol. 59, no. 1, pp. 145–159, Jan. 2011.

[66] G. Wang, J. Xin, J. Wang, N. Zheng, and A. Sano, "Subspace-based two-dimensional direction estimation and tracking of multiple targets," *IEEE Trans. Aerosp. Electron. Syst.*, vol. 51, no. 2, pp. 1386–1402, Apr. 2015.

[67] D. G. Luenberger, "Observing the state of a linear system," *IEEE Trans. Mil. Electron.*, vol. 8, no. 2, pp. 74–80, Apr. 1964.

[68] Y. Bar-Shalom and T. E. Fortmann, *Tracking and Data Association*. New York, Ny, USA: Academic Press, 1988.

[69] G. F. Franklin, J. D. Powell, and M. Workman, *Digital Control of Dynamic Systems*, 3rd ed. Boston, MA, USA: Addison-Wesley, 1998.

[70] W. Zuo, J. Xin, N. Zheng, and A. Sano, "Subspace-based localization of far-field and near-field signals without eigendecomposition," *IEEE Trans. Signal Process.*, vol. 66, no. 17, pp. 4461–4476, Sep. 2018.

[71] P. R. Singh, Y. Wang, and P. Chargé, "Performance enhancement of approximated model based near-field sources localisation techniques," *IET Signal Process.*, vol. 11, no. 7, pp. 825–829, 2017.

[72] E. Zhou, H. Jiang, and H. Qi, "4-D parameter estimation in bistatic MIMO radar for near-field target localization," in *Proc. IEEE Int. Wireless Symp.*, Shenzhen, China, Mar. 2015, pp. 1–4.

[73] P. R. Singh, Y. Wang, and P. Chargé, "Near field targets localization using bistatic MIMO system with symmetric arrays," in *Proc. 25th Eur. Signal Process. Conf.*, Kos Island, Greece, Aug. 2017, pp. 2468–2471.

[74] P. R. Singh, Y. Wang, and P. Chargé, "Bistatic MIMO radar for near field source localisation using PARAFAC," *Electron. Lett.*, vol. 52, no. 12, pp. 1060–1061, 2016.

[75] P. R. Singh, Y. Wang, and P. Chargé, "An exact model-based method for near-field sources localization with bistatic MIMO system," *Sensors*, vol. 17, 2017, Art. no. 723.

[76] P. R. Singh, Y. Wang, and P. Chargé, "Near field targets localization using bistatic MIMO system with spherical wavefront based model," in *Proc. 25th Eur. Signal Process. Conf.*, Kos Island, Greece, Aug. 2017, pp. 2408–2412.

[77] I. Podkurkov, L. Hamidullina, E. Traikov, M. Haardt, and A. Nadeev, "Tensor-based near-field localization in bistatic MIMO radar systems," in *Proc. 22nd Int. ITG Workshop Smart Antennas*, Bochum, Germany, Mar. 2018, pp. 1–8 .

[78] T.-J. Jung and K. Lee, "Closed-form algorithm for 3-D single-source localization with uniform circular array," *IEEE Antennas Wireless Propag. Lett.*, vol. 13, pp. 1096–1099, 2014.

[79] L. Zuo, J. Pan, and Z. Shen, "Analytical algorithm for 3-D localization of a single source with uniform circular array," *IEEE Antennas Wireless Propag. Lett.*, vol. 17, no. 2, pp. 323–326, Feb. 2018.

[80] M. N. El Korso, R. Boyer, A. Renaux, and S. Marcos, "Nonmatrix closed-form expressions of the Cramér–Rao bounds for near-field localization parameters," in *Proc. IEEE Int. Conf. Acoust., Speech, Signal Process.*, Taipei, Taiwan, Apr. 2009, pp. 3277–3280.

[81] M. N. El Korso, R. Boyer, A. Renaux, and S. Marcos, "Conditional and unconditional Cramér–Rao bounds for near-field source localization," *IEEE Trans. Signal Process.*, vol. 58, no. 5, pp. 2901–2907, May 2010.

[82] M. N. El Korso and M. Pesavento "Performance analysis for near field source localization," in *Proc. IEEE 7th Sens. Array Multichannel Signal Process. Workshop*, Hoboken, NJ, USA, Jun. 2012, pp. 197–200.

[83] T. Bao, M. N. El Korso, and H. H. Ouslimani, "Cramér–Rao bound and statistical resolution limit investigation for near-field source localization," *Digit. Signal Process.*, vol. 48, pp. 137–147, 2016.

[84] M. N. El Korso, A. Renaux, R. Boyer, and S. Marcos, "Deterministic performance bounds on the mean square error for near field source localization," *IEEE Trans. Signal Process.*, vol. 61, no. 4, pp. 871–877, Feb. 2013.

[85] Y. Begriche, M. Thameri, and K. Abed-Meraim, "Exact Cramér–Rao bound for near field source localization," in *Proc. 11th Int. Conf. Inf. Sci., Signal Process. Appl.*, Montreal, Canada, Jul. 2012, pp. 718–721.

[86] Y. Begriche, M. Thameri, and K. Abed-Meraim, "Exact conditional and unconditional Cramér–Rao bounds for near field localization," *Digit. Signal Process.*, vol. 31, pp. 45–58, 2014.

[87] J. P. Delmas and H. Gazzah, "CRB analysis of near-field source localization using uniform circular arrays," in *Proc. IEEE Int. Conf. Acoust., Speech, Signal Process.*, Vancouver, Canada, May 2013, pp. 3996–4000.

[88] J. P. Delmas, M. N. El Korso, H. Gazzah, and M. Castella, "CRB analysis of planar antenna arrays for optimizing near-field source localization," *Signal Process.*, vol. 127, pp. 117–134, 2016.

[89] S. Marcos and M. Benidir, "Source bearing estimation and sensor positioning with the propagator method," in *Proc. SPIE Adv. Signal Process. Algorithms, Archit., Implementations*, vol. 1348, San Diego, CA, USA, Jul. 1990, pp. 312–323.

[90] S. Marcos, A. Marsal, and M. Benidir, "Performance analysis of the propagation method for source bearing estimation," in *Proc. IEEE Int. Conf. Acoust., Speech, Signal Process.*, vol. 4, Adelaide, Australia, Apr. 1994, pp. 237–240.

[91] A. Marsal and S. Marcos, "A reduced complexity ESPRIT method and its generalization to antenna of partially unknown shape," in *Proc. IEEE Int. Conf. Acoust., Speech, Signal Process.*, vol. 4, Adelaide, Australia, Apr. 1994, pp. 29–32.

[92] S. Marcos and M. Benidir, "An adaptive subspace algorithm for direction finding and tracking," in *Proc. SPIE Adv. Signal Process. Algorithms, Archit., Implementations*, vol. 2563, Hong Kong, Jun. 1995, pp. 230–239.

[93] S. Marcos, M. Benidir, and J. Sanchez-Araujo, "An adaptive tracking algorithm for direction finding and array shape estimation in a nonstationary environment," *J. VLSI Signal Process. Syst.*, vol. 14, no. 1, pp. 107–118, 1996.

[94] J. Sanchez-Araujo and S. Marcos, "A class of subspace-based methods without eigendecomposition," in *Proc. IASTED Int. Conf. Signal Image Process. Appl.*, Annecy, France, Jun. 1996, pp. 202–205.

[95] S. Marcos and J. Sanchez-Araujo, "High resolution 'linear' methods for direction of arrival estimation: Performance and complexity," *Traitement du Signal*, vol. 14, no. 2, pp. 99–116, 1997.

[96] J. Sanchez-Araujo and S. Marcos, "Tracking moving sources using subspace-based adaptive linear methods," in *Proc. IEEE Int. Conf. Acoust., Speech, Signal Process.*, vol. 5, Munich, Germany, Apr. 1997, pp. 3497–3500.

[97] J. Sanchez-Araujo, and S. Marcos, "An efficient PASTd-algorithm implementation for multiple direction of arrival tracking," *IEEE Trans. Signal Process.*, vol. 47, no. 8, pp. 2321–2324, Aug. 1999.

[98] D. B. Ward and G. W. Elko, "Mixed nearfield/farfield beamforming: A new technique for speech acquisition in a reverberant environment," in *Proc. IEEE ASSP Workshop Appl. Signal Process. Audio Acoust.*, New Paltz, NY, USA, Oct. 1997, pp. 19–22.

[99] G. Arslan and F. A. Sakarya, "A unified neural-network-based speaker localization technique," *IEEE Trans. Neural Netw.*, vol. 11, no. 4, pp. 997–1002, Jul. 2000.

[100] P. Tichavsky, K. T. Wong, and M. D. Zoltowski, "Near-field/far-field azimuth elevation angle estimation using a single vector-hydrophone," *IEEE Trans. Signal Process.*, vol. 49, no. 11, pp. 2498–2510, Nov. 2001.

[101] J. Liang and D. Liu, "Passive localization of mixed near-field and far-field sources using two-stage MUSIC algorithm," *IEEE Trans. Signal Process.*, vol. 58, no. 1, pp. 108–120, Jan. 2010.

[102] J. He, M. N. S. Swamy, and M. O. Ahmad, "Efficient application of MUSIC algorithm under the coexistence of far-field and near-field sources," *IEEE Trans. Signal Process.*, vol. 60, no. 4, pp. 2066–2070, Apr. 2012.

[103] B. Wang, J. Liu, and X. Sun, "Mixed sources localization based on sparse signal reconstruction," *IEEE Signal Process. Lett.*, vol. 19, no. 8, pp. 487–490, Aug. 2012.

[104] J.-J. Jiang, F.-J. Duan, J. Chen, Y.-C. Li, and X.-N. Hua, "Mixed near-field and far-field sources localization using the uniform linear sensor array," *IEEE Sens. J.*, vol. 13, no. 8, pp. 3136–3143, Aug. 2013.

[105] K. Wang, L. Wang, J.-R. Shang, and X.-X. Qu, "Mixed near-field and far-field source localization based on uniform linear array partition," *IEEE Sens. J.*, vol. 16, no. 22, pp. 8083–8090, Nov. 2016.

[106] J.-J. Jiang, F.-J. Duan, and X.-Q. Wang, "An efficient classification method of mixed sources," *IEEE Sens. J.*, vol. 16, no. 10, pp. 3731–3734, May 2016.

[107] A. Renaux, R. Boyer, and S. Marcos, "Lower bounds on the MSE for mixed far-field and near-field sources direction-of-arrivals," in *Proc. IEEE 46th Asilomar Conf. Signals, Syst. Comput.*, Pacific Grove, CA, USA, Nov. 2012, pp. 18–22.

[108] C. W. Ma and C. C. Teng, "Tracking a near-field moving target using fuzzy neural networks," *Fuzzy Sets Syst.*, vol. 110, no. 3, pp. 365–377, 2000.

[109] D. K. Borah and A. Balagopal, "Localization and tracking of multiple near-field sources using randomly distributed sensors," in *Proc. IEEE 38th Asilomar Conf. Signals, Syst., Comput.*, vol. 1, Pacific Grove, CA, USA, 2004, pp. 1323–1327.

Hiromitsu Ohmori (M'88) received the B.E.E., M.E.E., and Ph.D. degrees from Keio University, Yokohama, Japan, in 1983, 1985, and 1988, respectively. In April 1988, he joined as the Instructor in the Department of Electrical Engineering, Keio University, Japan. In April 1991, he became the Assistant Professor with the same department. In April 1996, he became the Associate Professor with the Department of System Design Engineering, Keio University. He is currently a Professor with the same department. His research interests include the fields of adaptive control, robust control, nonlinear control, and their applications. He is the member of SICE, ISCIE, IEE, IEICE, EICA, etc.

Nanning Zheng (SM'93–F'06) graduated from the Department of Electrical Engineering, Xi'an Jiaotong University, Xi'an, China, in 1975, the M.S. degree in information and control engineering from Xi'an Jiaotong University, in 1981, and the Ph.D. degree in electrical engineering from Keio University, Yokohama, Japan, in 1985. In 1975, he joined Xi'an Jiaotong University, where he is currently a Professor and the Director with the Institute of Artificial Intelligence and Robotics. His research interests include computer vision, pattern recognition and image processing, and hardware implementation of intelligent systems. He became a member of the Chinese Academy of Engineering in 1999, and he is the Chinese Representative on the Governing Board of the International Association for Pattern Recognition. He also serves as an Executive Deputy Editor of the *Chinese Science Bulletin*.

Weiliang Zuo received the B.E. degree in electrical engineering and the Ph.D. degree in control science and engineering, from Xi'an Jiaotong University, Xi'an, China, in 2010 and 2018, respectively. During 2016–2017, he was a Visiting Student with the School of Electrical and Computer Engineering, Georgia Institute of Technology, Atlanta, GA, USA. Since 2019, he has been with Xi'an Jiaotong University. His research interests include array and statistical signal processing and pattern recognition.

Jingmin Xin (S'92–M'96–SM'06) received the B.E. degree in information and control engineering from Xi'an Jiaotong University, Xi'an, China, in 1988, and the M.S. and Ph.D. degrees in electrical engineering from Keio University, Yokohama, Japan, in 1993 and 1996, respectively. From 1988 to 1990, he was with the Tenth Institute of Ministry of Posts and Telecommunications, Xi'an, China. He was an Invited Research Fellow of the Telecommunications Advancement Organization of Japan with the Communications Research Laboratory, Tokyo, Japan, from 1996 to 1997, and a Postdoctoral Fellow with the Japan Science and Technology Corporation, from 1997 to 1999. He was also a Guest (Senior) Researcher with YRP Mobile Telecommunications Key Technology Research Laboratories Company, Limited, Yokosuka, Japan, from 1999 to 2001. From 2002 to 2007, he was with Fujitsu Laboratories Limited, Yokosuka, Japan. Since 2007, he has been a Professor with Xi'an Jiaotong University. His research interests include the areas of adaptive filtering, statistical and array signal processing, system identification, and pattern recognition.

Akira Sano (M'89) received the B.E., M.S., and Ph.D. degrees in mathematical engineering and information physics from the University of Tokyo, Tokyo, Japan, in 1966, 1968, and 1971, respectively. In 1971, he was with the Department of Electrical Engineering, Keio University, Yokohama, Japan, where he was a Professor with the Department of System Design Engineering till 2009. He is currently a Professor Emeritus with Keio University. He was a Visiting Research Fellow with the University of Salford, Salford, U.K., from 1977 to 1978. He is a coauthor of the textbook *State Variable Methods in Automatic Control* (Wiley, 1988). His research interests include adaptive modeling and design theory in control, signal processing and communication, and applications to control of sounds and vibrations, mechanical systems, and mobile communication systems. He has been a member of Science Council of Japan, since 2005. He was the recipient of the Kelvin Premium from the Institute of Electrical Engineering, in 1986. He is a Fellow of the Society of Instrument and Control Engineers and is a member of the Institute of Electrical Engineering of Japan and the Institute of Electronics, Information and Communications Engineers of Japan. He was the General Co-Chair of 1999 IEEE Conference of Control Applications and an IPC Chair of 2004 IFAC Workshop on Adaptation and Learning in Control and Signal Processing. He served as the Chair of IFAC Technical Committee on Modeling and Control of Environmental Systems from 1996 to 2001. He has also been the Vice Chair of IFAC Technical Committee on Adaptive Control and Learning since 1999 and has been the Chair of IFAC Technical Committee on Adaptive and Learning Systems since 2002. He was also on the Editorial Board of *Signal Processing*.